Adv. Theor. Math. Phys. **12** (2008) 489–545

Dimer models from mirror symmetry and quivering amoebæ

Bo Feng[1,2], Yang-Hui He[3,4], Kristian D. Kennaway[5], and Cumrun Vafa[6]

[1]Blackett Laboratory, Imperial College, London, SW7 2AZ, UK
[2]The Institute for Mathematical Sciences, Imperial College London, 48 Princes Gardens, London SW7 2AZ, UK
[3]Merton College, Merton St., Oxford, OX1 4JD, UK
[4]Mathematical Institute, University of Oxford, 24-29 St. Giles', Oxford, OX1 3LB, UK
[5]Department of Physics, University of Toronto, Toronto, ON M5S 1A7, Canada
[6]Jefferson Physical Laboratory, Harvard University, Cambridge, MA 02138, USA
b.feng@cms.zju.edu.cn
yang-hui.he@merton.ox.ac.uk
kennaway@ihes.fr
vafa@string.harvard.edu

Abstract

Dimer models are 2-dimensional combinatorial systems that have been shown to encode the gauge groups, matter content and tree-level superpotential of the world-volume quiver gauge theories obtained by placing D3-branes at the tip of a singular toric Calabi–Yau cone. In particular the dimer graph is dual to the quiver graph. However, the string theoretic explanation of this was unclear. In this paper we use mirror symmetry to

e-print archive: http://lanl.arXiv.org/abs/hep-th/0511287v1

shed light on this: the dimer models live on a T^2 subspace of the T^3 fibre that is involved in mirror symmetry and is wrapped by D6-branes. These D6-branes are mirror to the D3-branes at the singular point, and geometrically encode the same quiver theory on their world-volume.

Contents

1 Introduction

Non-compact Calabi–Yau 3-folds corresponding to toric geometries have been a source of many interesting insights for string theory, including geometric engineering, local mirror symmetry, topological strings and large N dualities. One important question in this context is how one describes the gauge theory living on a D3-brane placed at a singular point of a toric 3-fold.

Some special cases of this correspondence have been understood for a while [1–8]. More recently it was shown that dimer models on T^2 encode the full data of the quiver gauge theory [9, 10]. This simple picture led to a number of new insights [11–15]. However, a direct explanation of the relevance of the dimer models as systems deriving from string theory was unclear. This link between dimer models and the quiver gauge theory from toric geometries must have a more direct explanation. This is because it has been well known that dimer models are naturally associated to toric geometries (see [16] for a discussion of this point).

The problem we will address in this paper is to understand the relation of the dimer models to string theory and their relation to previous geometrical constructions of quivers [4]. Following [3], we use mirror symmetry to relate the D3-brane to a system of intersecting D6-branes in the mirror geometry. These are mirror to the wrapped branes on the exceptional cycle of the singular geometry, which carry the gauge groups of the quiver theory, and whose pattern of intersection encode the bifundamental matter of the quiver via the massless strings localized at their intersection points. We propose that the geometry of the mirror D6-branes, which by mirror symmetry should correspond to T^3, are further divided up to a number of intersecting S^3s. Moreover, this collection of S^3s admit a projection to a $T^2 \subset T^3$, with fibre being an S^1. This projection gives a certain tiling of T^2 where the boundary of faces are identified with loci where the fibre S^1 vanishes. This tiling of the T^2 is the dimer model!

We explain how the geometry of the mirror D6-branes induces the "rules" of the dimer models on T^2, in particular why the dimer models encode the gauge groups, matter content and tree-level superpotential of the quiver theory coming from the D6-brane intersections. Specifically, matter arises from the intersection loci of the D6-branes wrapping S^3s and superpotential terms arise when a collection of D6-branes meet at a point. This will explain the origin of the dimer model and the way it encodes the quiver gauge theory.

1.1 Setup and organization

We study the physics living on the world-volume of D3-branes probing transversely a toric Calabi–Yau 3-fold $\mathcal{M}$. The theory is a gauge theory whose matter content is summarized in a *quiver diagram*. One applies local mirror symmetry and translates this setup to D6-branes wrapping Lagrangian T^3 in the mirror Calabi–Yau 3-fold $\mathcal{W}$. We will chiefly work in the mirror manifold $\mathcal{W}$. The intersection of the 3-cycles in $\mathcal{W}$ gives the spectrum corresponding to the quiver. This is, by now, a standard construction [3, 4, 6, 17]; however, we will propose a more detailed description which we will summarize in Section 3.

The organization of the paper is as follows. In Section 2 we review some relevant aspects of mirror symmetry as applied to toric 3-folds. In Section 3 we discuss the general structure of our proposal. In Section 4 we discuss some facts about dimer models and local toric 3-folds. We then analyse how one lifts the dimer model from T^2 to a graph on a Riemann surface in Section 5; this constitutes a central idea of our proposal. In Section 6 we discuss projections of the local mirror geometry on the base of the mirror

fibration (the so-called 'amoebae') as well as the $T^2 \subset T^3$ of the mirror fibre (the so-called 'algae'). Finally, in Section 7 we discuss how dimer models arise from Algae and also how our proposal is concretely realized through examples. We conclude with prospects in Section 8 and in Appendix A, we give some mathematical results on Newton polytopes and critical points.

2 Toric geometry and mirror symmetry

In this section we discuss aspects of mirror symmetry in the context of local toric 3-folds following the derivation in [18] and its application to the study of mirror of the D-branes discussed in [3]. For a review of toric geometry and mirror symmetry see, e.g., [19].

Local toric 3-folds $\mathcal{M}$ are specified by a convex integer sublattice $Q \subset \mathbb{Z}^2$ (the so-called *toric diagram*). Our D3-branes probe the tip of this singular $\mathcal{M}$. It was shown in [18] (see also [3]) that the mirror geometry corresponding to it is given by a local 3-fold $\mathcal{W}$ specified by

$$W = P(z,w) := \sum_{(p,q)\in Q} c_{(p,q)} z^p w^q, \tag{2.1}$$

$$W = uv, \tag{2.2}$$

where w, z are $\mathbb{C}^*$ variables and u, v are $\mathbb{C}$ variables. The coefficients $c_{(p,q)}$ are complex numbers and are mirror to the Kähler moduli of the local toric geometry. Three of the $c_{(p,q)}$s can be set to 1 by rescaling of the variables. The mirror manifold $\mathcal{W}$ is therefore a double fibration over the W-plane. Even though W can be eliminated to give the local geometry $P(z,w) - uv = 0$, it is convenient for us to view it as a double fibration over the W-plane. We exemplify this in the diagram below, where we draw the toric diagram of the Hirzebruch surface $\mathbb{F}_0 \simeq \mathbb{P}^1 \times \mathbb{P}^1$; the Calabi–Yau 3-fold $\mathcal{M}$ is the affine cone over this surface:

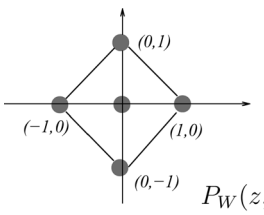

$$P_W(z,w) = c_{(0,0)} + c_{(0,1)} w + c_{(0,-1)} \tfrac{1}{w} + c_{(1,0)} z + c_{(-1,0)} \tfrac{1}{z} \tag{2.3}$$

Out of the five cs three can be set to 1 and the other two are mirror to Kähler moduli of the two $\mathbb{P}^1$s. Another terminology to which we shall later refer is that we call the interior lattice point(s) in the toric diagram (such as the point $(0,0)$ in (2.3)) the *internal point(s)* and those on the boundary,

the *external points.* The number of internal points will turn out to be very important to us.

The T^3 symmetry, denoted by three phases (α, β, γ) which is used in the mirror symmetry derivation (in accord with the conjecture [20]) act on the geometry as

$$\begin{aligned} z &\to \alpha z \\ w &\to \beta w \\ u/|u| &\to \gamma u/|u| \end{aligned} \tag{2.4}$$

(the action on v is specified by requiring that $P(z, w) - uv = 0$ remain valid). Since $u \in \mathbb{C}$, the circle action on u degenerates when $u = 0$. In particular the T^3 mirror fibre can be viewed as fibred over the $(\alpha, \beta) \in T^2$ with an S^1 fibre which degenerates at $u = 0$, i.e., at loci where $P(z, w) = 0$.

2.1 The curve $P(z,w) = W$ and D6-branes

We are now ready to describe the mirror D6-branes and its relation to the T^3 geometry described above, following [3]. The most important equation, which encodes the essential content of the toric geometry, is the curve $P(z, w) = W$, the study of which shall be our primary concern. The definition (2.1) dictates that $P(z, w)$ is the *Newton polynomial* associated with the toric diagram; conversely, the diagram is the *Newton polytope*[1] for the polynomial $P(z, w)$. These concepts are widely used in combinatorial geometry. The coefficients $c_i \in \mathbb{C}^*$, which parametrize the complex structure deformations of $\mathcal{W}$, correspond to Kähler deformations of the mirror $\mathcal{M}$. For our example in (2.3), the Newton polynomial for the associated toric diagram of $\mathbb{F}_0$ is indicated.

Now, this curve $P(z, w) - W = 0$ is a genus g (punctured) *Riemann surface*, which we will denote as Σ_W, fibred over each point W. The genus is prescribed by the simple relation [21, 22]

$$g = \text{number of internal points in the toric diagram.} \tag{2.5}$$

Of particular importance to us is the fibre above the origin, $P(z, w) = 0$, which we call Σ.

[1]Strictly, the Newton polytope is the convex hull of the lattice points of exponents. Here, since our original toric data is itself a convex polytope, the hull over $\mathbb{Z}$ is simply the toric points themselves.

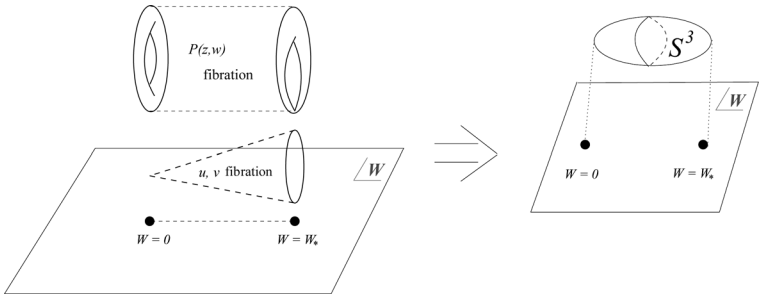

Figure 1: The geometry of the mirror of the toric 3-fold $\mathcal{M}$. It is here shown explicitly as a double fibration over the W-plane: one being a circle $W = uv$ degenerating at $W = 0$ and another being a fibration of a Riemann surface Σ defined by $W = P(z, w)$ degenerating at critical points $W = W_*$. Together the two fibrations constitute 3-spheres over lines joining 0 and W_*.

Whenever we are at a critical point of $P(z, w)$, given by

$$(z_*, w_*) \text{ s.t. } \left(\frac{\partial}{\partial z}P(z,w) = \frac{\partial}{\partial w}P(z,w) = 0\right)\Big|_{(z_*,w_*)}, \tag{2.6}$$

or, in the W-plane, over the point $W_* = P(z_*, w_*)$, a cycle in Σ_W degenerates and pinches off. On the other hand, the point $W = 0$ is, as mentioned above, special in that here the S^1-fibre governed by u, v pinches. We may therefore join, by a straight line, $W = 0$ to each of the critical points W_* with a fibre which is an $S^1 \times S^1$; at the $W = 0$ one S^1 shrinks and at $W = W_*$ an $S^1 \subset \Sigma$ degenerates. The total space over this interval thus has the topology of an S^3. We illustrate this structure in figure 1. These S^3s form a basis $\{S_i\}$ for $H^3(\mathcal{W}; \mathbb{Z})$ and thus the T^3 class can be expanded therein as

$$\left[T^3\right] = \sum_i a_i S_i. \tag{2.7}$$

2.1.1 D6-branes wrapping the T^3-class

The D6-branes wrap the S^3-classes in (2.7) and therefore will intersect one another in the fibre above the origin where all the S^3 meet. This is shown in figure 2. The graph Γ where the intersection takes place is of great significance and will be explained in detail in Section 5. Equation (2.6) tells us that the number of D6-branes, which should be the number of gauge groups in the quiver theory, should be equal to the number of critical points of $W = P(z, w)$, In fact, it was pointed out in [3] that the matter content of the quiver theory is actually captured by the soliton spectrum of a 2-dimensional $\mathcal{N} = (2, 2)$ Landau–Ginzburg (LG) theory with superpotential $W = P(z, w)$.

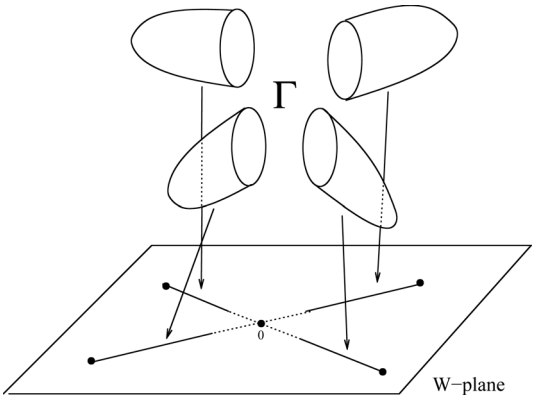

Figure 2: Above each straight-line path from the critical point of W to $W = 0$ the vanishing cycle in the fibre $P(z, w) = W$ sweeps out a disc. Above the origin the boundaries of these discs (hats) intersect the fibre $P(z, w) = 0$ along some graph Γ. Not shown is the other S^1 fibre, which vanishes above the origin and is non-trivial elsewhere. The total space of each path is an S^3 in the mirror geometry.

We show in Appendix A that $W = P(z, w)$ has the correct number of critical points to produce the basis of wrapped D6-branes as long as the genus of the curve $P(z, w) = 0$ is greater than 0 (i.e., the toric diagram contains 1 or more internal point). This number of critical points is equal to twice the area of the toric diagram, which is in turn equal to the number of gauge groups in the quiver, as it should. This is equivalent to saying that the original geometry $\mathcal{M}$ contains a vanishing 4-cycle. If it contains only vanishing 2-cycles (such as the conifold), then the mirror curve has genus 0 and we seem not to obtain enough critical points from $W = P(z, w)$ to describe the basis of D6-branes of the quiver theory.

Thus it appears that the description of the mirror geometry as a fibration over the W-plane is best suited to the case of vanishing 4-cycles, and there may exist another presentation better suited to the case of vanishing 2-cycles. This is related to the fact that $W = P(z, w)$ is the superpotential of the massive LG model mirror to a sigma model with target space given by the 4-cycle. In the vanishing 2-cycle cases, it suggests that there should be a way to relate the mirror geometry to the LG model mirror to the 2-cycle. However, even in the case of vanishing 2-cycle, we are still able to obtain the full data of the quiver theory[2] from intersections of 1-cycles on the curve $P(z, w) = 0$. Thus, the majority of our results hold in generality.

[2]When the curve has genus 0 the resulting quiver is always *non-chiral*, an observation which does not appear to have been made before.

2.2 Toric diagrams and (p,q)-webs

Let us investigate the above picture from another well-known perspective, namely that of (p,q)-webs. The field theory associated with the (p,q)-webs was studied in [23], where (p,q) refers to a 5-brane, with $(1,0)$ being the D5-brane and $(0,1)$ being the NS5-brane. Suppressing 3 of the transverse directions thus represents our branes as intersections of lines in a 2-dimensional coördinate system with axes (p,q) so that the charge of the (p,q) 5-brane is aligned to its slope. These configurations are the so-named (p,q)**-webs** of 5-branes. Thus 5-branes are associated to edges in the web; one too could associate D3-branes with vertices and D7-branes with faces. In other words, the web, though generated from a 5-dimensional theory, essentially corresponds to D3, D5 and D7-branes wrapping 0, 2 and 4-cycles, respectively, in $\mathcal{M}$, resulting in an encoding of the original quiver gauge theory living on the world-volume of the D3-brane probe.

It was shown in [24] that this web of 5-branes is S-dual to M-theory on a toric Calabi–Yau 3-fold. Moreover,

> *The (p,q) web diagram is the graph dual of the toric diagram of $\mathcal{M}$.*

This is really because there is a special Lagrangian $T^2 \times \mathbb{R}$ fibration of $\mathcal{M}$, where the (p,q)-cycle of T^2 vanishes along the corresponding edge of the web. The vanishing cycles turn into the 5-branes using S-dualities. In fact, the Riemann surface Σ defined by $P(z,w)=0$ can be thought of as a thickening of the (p,q)-web. We will make this statement clear in Section 6.1.1. For now, let us illustrate the above discussion in figure 3. For our example of F_0 presented in (2.3), we draw the corresponding (p,q)-web in figure 3(b) by

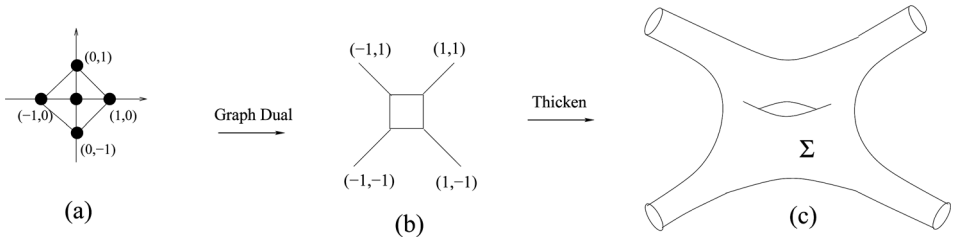

Figure 3: (a) The toric diagram of F_0; (b) the corresponding (p,q)-web as a graph dual, with the charges marked; (c) the Riemann surface $P(z,w)=0$ defined by the Newton polynomial of (a) is a thickening of (b); far away it looks like cylinders and in the interior it has holes depending on the number of internal points in (a).

graph dualizing the toric diagram which we redraw in part (a). In part (c) we draw the Riemann surface Σ defined by $P(z, w) = 0$ and see that it is a thickening of the (p, q)-web; the punctures correspond to the legs while the handle corresponds to the internal point. Far away along the (p, q)-directions Σ looks like cylinders.

In the case of the toric diagram having one internal point [3, 4], the antisymmetric part of the adjacency matrix of the quiver, i.e., the topological intersection number, $S_i \circ S_j$, is given by a simple expression. In terms of the (p, q)-charges of the legs, it is

$$A_{ij} = S_i \circ S_j = \det \begin{pmatrix} p_i & p_j \\ q_i & q_j \end{pmatrix}, \tag{2.8}$$

which we see to be explicitly antisymmetric due to the determinant. This formula does not hold for more than one internal point. However, the total number of fields in the quiver given by

$$N_f = \frac{1}{2} \sum_{i,j \in \text{ legs}} \left| \det \begin{pmatrix} p_i & q_i \\ p_j & q_j \end{pmatrix} \right| \tag{2.9}$$

still holds for at least one phase of the quiver theory. The reason for this is different though. As we explain later, we will relate these (p, q) charges to some auxiliary curves (so-called zig-zag paths) instead of the S^3-basis in (2.7). Then, the formula (2.9) counts the total topological intersection number among these curves. All matter fields will be in 1-1 correspondence with the intersection of these auxiliary curves.

3 Our general proposal

Having reviewed the requisite knowledge and the various inter-relations amongst them, we are now at a position to discuss our proposal in detail. Our general strategy is very simple: we are interested in studying the gauge theory on N D3-branes filling the $(3 + 1)$-dimensional spacetime, and placed at the tip of a singular locus of a toric Calabi–Yau 3-fold $\mathcal{M}$. Since there are world-sheet instanton corrections to the geometry of toric 3-folds, it is natural to use mirror symmetry where the classical geometry is reliable. In this context we can study what gauge theory lives on the mirror of the D3-brane.

The mirror of the N D3-branes will be N D6-branes filling the spacetime and wrapping the mirror of a point. The mirror of a point will be a T^3 inside a Calabi–Yau $\mathcal{W}$. For a generic point inside the Calabi–Yau, the mirror of a point would be a smooth T^3 and thus the mirror geometry would be the maximally supersymmetric $U(N)$ gauge theory in $(6 + 1)$ dimensions,

reduced on a T^3 to $(3+1)$ dimensions. However, we are interested in placing the D3-brane at a singular locus of the toric 3-fold. Clearly as we vary the point where the D3-brane is placed the fact that the mirror is a T^3 does not change. However, what may happen is that at special points the T^3 degenerates — similar to the degenerations familiar for a T^2, where it can become pinched. For example T^2 can get pinched to a bunch of S^2s joined back to back.

A similar thing is happening here for the T^3: placing N D3-branes at the singular point is the mirror image of N D6-brane's wrapping a singular T^3 made up of a collection of intersecting S^3s. The reduction of N D3-branes on S^3 gives rise to an $\mathcal{N}=1$, $U(N)$ gauge theory in 4 dimensions. So if we have the T^3 being made up of k component S^3s, we will have a theory with a gauge group $G=U(N)^k$.

Furthermore, the S^3s intersect one another. If they intersect over an S^1 then we get a massless bifundamental hypermultiplet $(N,\overline{N})$ between the corresponding $U(N)$s. However, in the cases discussed here we find that they intersect not over S^1s but over intervals. Since two intervals glued back to back make up an S^1, we should be getting half of a hypermultiplet from an interval, i.e., an $\mathcal{N}=1$ chiral $(N,\overline{N})$ multiplet. Furthermore, if a number of S^3s intersect at a point, i.e., where the intervals meet, then there would be world-sheet disc instantons which get mapped to the intersection point of the S^3s and can give rise to a superpotential for the corresponding chiral multiplets. The result, is an $\mathcal{N}=1$ quiver gauge theory in 4 dimensions, which is the familiar world-volume theory of the D3-brane probe [1].

In order to flesh out the scenario presented in Section 1.1, we will have to find a convenient way of encoding the intersecting geometry of the S^3s that make up the T^3. We recall that it is the T^3 which the D6-branes wrap, and the intersection of the S^3s give the quiver matter content of our gauge theory. Our proposal will be to demonstrate intimate connections between the mirror geometry, especially the Riemann surface Σ and a certain corresponding dimer model the general properties of which we review in the next section.

Specifically, we will show that in the fibre Σ above $W=0$ (which we recall is given by the equation $P(z,w)=0$) there exists a graph Γ that admits non-trivial 1-cycles with the correct properties to encode the gauge groups and matter content of the quiver theory. Thus, Γ describes the intersection of the D6-branes with the curve Σ (cf. figure 2).

Next, we need to show how the intersecting D6-branes map to a $T^2\subset T^3$. This T^2 is embedded in the geometry according to mirror symmetry, and we will exhibit it in two ways.

Mapping S^3 to Discs on T^2. Firstly, we describe a map between the intersection of the S^3s with the curve Σ, and a graph on T^2. This T^2 is *topologically* identified with the $T^2 \subset T^3$ of the D6-brane world-volume. We will find that the S^3s map to polygons (topologically, discs) that span the entire T^2, and join up along the graph of a certain dimer model. The remaining circle of the T^3 is fibred over the T^2 so that it vanishes precisely along this graph, i.e., the intersection locus of Σ with this T^2.

Moreover, we find that the discs intersect on intervals. Thus the intervals, i.e., the edges of the graph obtained by the intersection of $P(z, w) = 0$ with the T^2, give rise to bifundamental chiral multiplets. Furthermore, the vertices of the dimer model, which correspond to specific points on T^2 give rise to superpotential, via open string disc instantons attached to the vertices.

One may read off the superpotential by going around the boundary of the disc, which is a circle around the vertex of the graph and writing the corresponding chiral multiplet associated with each edge, the circle intersects in an ordered fashion. Furthermore, there is a sign associated to the generated superpotential term. It is easy to see that it has to be there: vertices which are the boundary of a given edge give rise to opposite signs for the superpotential contribution.

In order to argue for this, a heuristic reasoning is as follows: Suppose we have an S^1 intersection region which can be *artificially* divided to two intervals, from each of which we obtain a chiral multiplet: $X : (N, \overline{N})$ and $\tilde{X} = (\overline{N}, N)$. Then we will get superpotential terms from the two vertices proportional to $TrX\tilde{X}$ and $Tr\tilde{X}X$. If they come with the same phase these two terms will add and would correspond to a massive hypermultiplet. However, we know that the theory with an S^1 intersection must give rise to a massless hypermultiplet, therefore these two terms should come with opposite phases. So if we normalize the field so one of them comes with a $+$ sign, the other one should come with a $-$ sign so they would cancel.

Projections: Realizing the T^2 concretely. Secondly, we also find that in suitable cases the T^2 of the dimer model may be obtained by projecting (the so-called alga projection which we will discuss in Section 7) the S^3s onto the $T^2 \subset T^3$ defined by the phases of (z, w) in our local model. This gives a concrete embedding of the T^2 into the geometry.

Since these D6-branes (faces of the dimer model) together span the entire T^2 and the transverse S^1 that vanishes over the locus of the dimer model graph within this T^2, we have identified the singular T^3 that is mirror to the D3-brane at the singular point of the toric Calabi–Yau 3-fold $\mathcal{M}$.

4 Dimer models and quiver gauge theories

We have reviewed the mirror geometry for toric 3-folds as well as (p, q)-webs, the last requisite ingredient to our story are the dimer models. In this section, we review some relevant properties concerning dimer models [25, 26] and then review their recently uncovered combinatorial relation to gauge theories [9, 10, 14].

4.1 Some rudiments on dimer models

Let us start with some basic terminologies. A *bipartite graph* is a graph with the property that all vertices can be divided into black or white, such that every black vertex is only adjacent (i.e., linked by an edge) to white vertices, and vice versa. A *perfect matching* of a bipartite graph is a subset of edges such that every vertex in the graph is an endpoint of precisely one such edge. To the chemist, the matching consists of white–black pairs ("dimers") linked by a single edge (bond). To the mathematical physicist, a *dimer model* is the statistical mechanics of such a system, viz., a system of random perfect matchings of the bipartite graph with some appropriately assigned weights for the edges.

In principle, dimer models can be discussed with arbitrary boundary conditions, but the one in which we are particularly interested are graphs on oriented Riemann surfaces. In fact, two such Riemann surfaces will be relevant to us: one is the torus T^2 and the other is Σ defined by $P(z, w) = 0$. We will discuss dimer models on T^2, and later, isomorphic dimer models on Σ.

Many important properties of the dimer models are encoded in the *Kasteleyn matrix* $K(z, w)$ [27]. It is a weighted adjacency matrix of the graph with (in our conventions) the rows indexed by the white nodes, and the columns indexed by the black nodes constructed by the following rules:

1) Associate, to each edge, a number e_i called the *edge weight*. In previous literature on dimer models, the e_i were taken to be real and subject to a constraint on the parity of the product of edges around the faces of the dimer model. We shall see later than it is natural for us to take e_i to be $\mathbb{C}^*$-valued, and not to impose any sign constraint.
2) Now, for dimer models defined on T^2, because there are two non-trivial cycles $(0, 1)$ and $(1, 0)$ on the torus, we can introduce two complex variables z, w to count their non-trivial effects by assigning them as weights on edges. The way of doing it is following. First, the colouring of vertices in the graph induces an orientation to the edges, for example,

choose the orientation "black" to "white." Second, we can construct paths γ_w, γ_z in T^2 that wind once around the $(0,1)$ and $(1,0)$ cycles of the torus, respectively. Such paths would cross the graph edges: for every edge crossed by γ_w, multiply the edge weight by a factor of w or $1/w$ (similarly for γ_z, one multiplies by z or $1/z$) according to the relative orientation of the edge crossed by γ.

The adjacency matrix of the graph weighted by the above factors is the Kasteleyn matrix $K(z,w)$ of the graph. The determinant of this matrix $P(z,w) = \det K$ is called the *characteristic polynomial* of the graph, and defines a *spectral curve* via $P(z,w) = 0$. The astute reader may with foresight see why we have named this curve as P; indeed later on it will be identified with the mirror curve in (2.1). The fact that dimer models implicitly know about local mirror symmetry may be taken as a hint that mirror symmetry should be involved in their string theoretical realization.

To make these above concepts concrete, let us present an illustrative example. This is actually the theory of the so-called phase-1 of the cone over the zeroth Hirzebruch surface $F_0 \simeq \mathbb{P}^1 \times \mathbb{P}^1$ (cf. [10, 7]) with the toric diagram and the Newton polynomial given in (2.3):

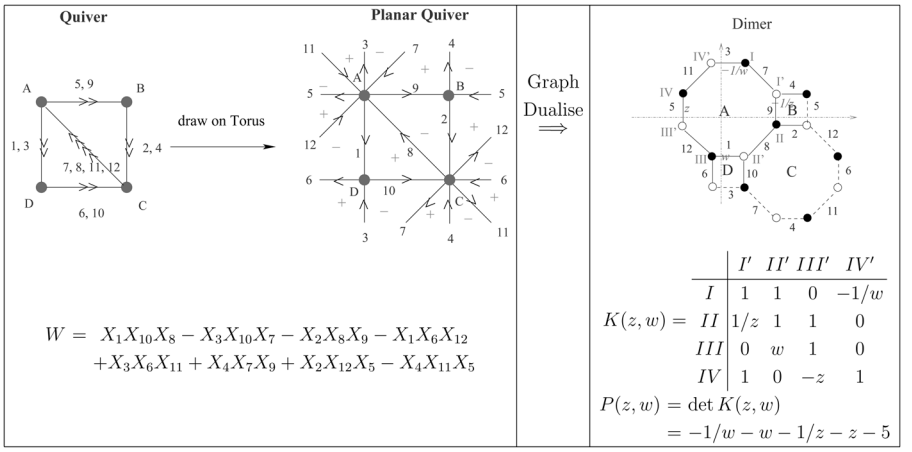

$$W = X_1X_{10}X_8 - X_3X_{10}X_7 - X_2X_8X_9 - X_1X_6X_{12} + X_3X_6X_{11} + X_4X_7X_9 + X_2X_{12}X_5 - X_4X_{11}X_5$$

$$K(z,w) = \begin{array}{c|cccc} & I' & II' & III' & IV' \\ I & 1 & 1 & 0 & -1/w \\ II & 1/z & 1 & 1 & 0 \\ III & 0 & w & 1 & 0 \\ IV & 1 & 0 & -z & 1 \end{array}$$

$$P(z,w) = \det K(z,w) = -1/w - w - 1/z - z - 5$$

(4.1)

In fact, $P(z,w)$ can be calculated by another way. Taking an arbitrary perfect matching M_0 on the graph as a reference and another perfect matching M, we can get a set of closed curves in the graph using the difference $M - M_0$. This in turn defines a *height function* on the faces of the graph: when a path (non-trivial cycle on T^2) crosses the curve, the height is increased or decreased by 1 according to the orientation of the crossing.

In terms of the height function, the characteristic polynomial takes the following form:

$$P(z,w) = z^{h_{x0}} w^{h_{y0}} \sum c_{h_x,h_y} (-1)^{h_x+h_y+h_x h_y} z^{h_x} w^{h_y} \tag{4.2}$$

where c_{h_x,h_y} are integer coefficients that count the number of paths on the graph with height change (h_x, h_y) around the two fundamental cycles of the torus. It is precisely due to (4.2) that the spectral curve is useful to the statistics of dimer models: the function $P(z,w)$ is the generating function for the perfect matchings M, counted according to the winding number of $M - M_0$.

The similarity between (4.2) and the Newton polynomial in (2.2) was one of the initial inspirations that led to the investigation of the correspondence between toric gauge theories and dimer models. We point out, however, that the coefficients in (2.2) are arbitrary complex parameters while those in (4.2) are integers. We need general moduli in order to make the dimer model explore the full Calabi–Yau geometry A. Craw, R. Karp and K. Kennaway, Work in progress.

Let us make some final remarks on the construction of $K(z,w)$ and $P(z,w)$. There is a freedom in the choice of paths γ_z, γ_w as well as the reference matching M_0. This freedom may result in different overall factors $z^{i_0} w^{j_0}$ in front of $P(z,w)$, and an $\mathrm{SL}(2,\mathbb{Z})$ transformation of the Newton polytope. This should not trouble us since for the Newton polytope (toric diagram) both transformations are induced by $\mathrm{SL}(3,\mathbb{Z})$ transformations of the lattice $\mathbb{Z}^3$, which does not effect the underlying geometry. Moreover, with the above choices of edge weights in the construction of $K(z,w)$, the coefficients c_{h_x,h_y} in $P(z,w)$ are integers (as they were originally devised by [27] as a counting problem).

However, as we shall identify $P(z,w)$ with the definition fibration of a mirror geometry, in order to account for the full moduli of the geometry,[3] it is preferable to have the edge weights, and hence c_{h_x,h_y}, to be arbitrary complex numbers, modulo the gauge degree of freedom corresponding to multiplying the weights of all edges incident to a given vertex by the same factor.

[3]It is also necessary to impose the D-term constraints coming from the linear sigma model, which restrict the moduli space of the world-volume theory to the geometrical phases [2].

4.2 Relation to toric gauge theories

Having reviewed the basics of dimer models, we continue recalling what has already been spelled out in recent literature on the relationship between dimer models and toric gauge theories [9, 10, 14].

It is observed that for toric gauge theories, that is, the setup discussed in Section 2 of placing D3-brane probes transverse to a toric Calabi–Yau singularity, there are some special properties. First, it is a quiver theory. This means that every matter field carries only two gauge indices, i.e., they are only charged under two gauge groups, as the fundamental of one and the antifundamental of another. Therefore, we can represent the matter content in terms of a finite graph called the quiver diagram, where vertices denote gauge groups, and edges the bifundamental matter fields [1].

Second, and this is special to toric singularities, every matter field shows up two and only two times in the superpotential, *one with plus sign and one with minus sign.* This was referred to as the "toric condition" in [8]. Furthermore, for *any* toric theory one may normalize the coefficient of each term in the superpotential to 1 by a rescaling of the fields. This is associated to the fact that after blowing up the toric singularity (i.e., deforming the Kähler moduli away from the singular point), there are no complex structure deformations of the resulting non-singular Calabi–Yau manifold, and these complex structure deformations would have shown up as coupling constants in W. It is only for non-toric singularities that one finds coupling constants that cannot be normalized away (e.g., for the non-toric del Pezzo cones, see [5]).

Now, every monomial term in the superpotential is gauge-invariant, which means that in the quiver diagram it corresponds to a closed path, traced by the edges (matter fields constituting this term) according to the order of gauge group index contractions. Combining this fact and the toric condition, it is easy to see that if we think of the superpotential terms as defining the boundary of *polygonal faces*, we can glue these faces (superpotential terms) together along their common edges to construct a tiling of an oriented Riemann surface without boundary, dubbed the "periodic quiver" in [10, 14]. Furthermore, every face can be assigned a plus or a minus, according to the sign of the term in the superpotential.

If we take the *planar dual graph of the periodic quiver*, that is, faces, edges, vertices are mapped to vertices, edges, faces, respectively, we obtain a bipartite graph. In other words, *the planar graph dual of the periodic quiver is a dimer model on a Riemann surface.*

Finally, it can be shown [10] that the superconformal conditions for toric gauge theories, viz., the R-charge of every term in superpotential must be 2 and the beta-function of every gauge group must be 0, imply the relation

$$F + V - E = 0. \tag{4.3}$$

Here, F, V, E are the numbers of faces, vertices and edges, respectively, in the periodic quiver diagram. Equivalently, they are the numbers of superpotential terms, gauge groups and bifundamental matter fields, respectively, in the gauge theory. Of course, (4.3) is the famous Euler relation, $F + V - E = 2 - 2g$. Thus, $g = 1$, and our periodic quiver actually lives on a torus T^2.

Now let us use one simple example to demonstrate the above procedure. The famous $\mathcal{N} = 4$ SU(N) theory has the superpotential, in $\mathcal{N} = 1$ language, $\mathrm{Tr}(X_1X_2X_3 – X_1X_3X_2)$. This is the theory of D3-branes probing the flat space $\mathbb{C}^3$. It is easy to construct the periodic quiver as shown in figure 4, where after we identify edges X_2 and X_3 we get a torus. Since there is only one black node and one white node, the K-matrix is a one-by-one matrix, with three monomial terms in z, w; this defines the toric data, as required.

In the dimer model, vertices correspond to superpotential terms. By multiplying every edge around a vertex by a common factor, the normalization of each term in the superpotential can be fixed to 1 as discussed above. Since this operation corresponds to multiplying a row or column of the Kasteleyn matrix by a common factor, it amounts to rescaling the determinant $P(z, w)$, which is a gauge transformation that does not affect the physics of the dimer model.

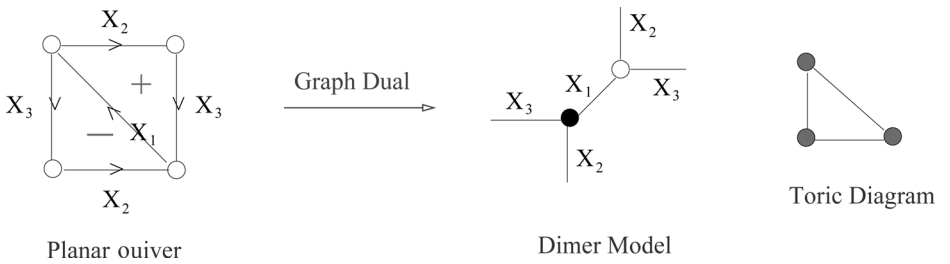

Figure 4: The planar periodic quiver for the theory on D3-branes on $\mathbb{C}^3$, i.e., the famous, $\mathcal{N} = 4$ theory has one gauge group SU(N) and superpotential $\mathrm{Tr}(X_1X_2X_3 – X_1X_3X_2)$. Its graph dual is a dimer model with just one pair of nodes. The toric diagram consist of the lattice points $\{(0, 0), (1, 0), (0, 1)\}$ and we have included it on the right. Indeed we can read out the toric diagram from the Kasteleyn matrix of the dimer model.

4.2.1 Summary: dimer models and quiver theories

Combining the above facts, we summarize the relation thus far known between dimer models and toric quiver gauge theories:

(a) Every toric gauge theory can be encoded into a *periodic quiver diagram* living on T^2 where gauge groups are represented by vertices, matter fields by edges, and superpotential terms by faces;
(b) The planar dual of the periodic quiver diagram is a bipartite graph, where now gauge groups are represented by faces, matter fields by edges, and superpotential terms with plus (minus) sign, by white (black) vertices.
(c) The dimer model on this bipartite graph is equivalent to the linear sigma model description of the world-volume quiver theory on the D3-branes [2]. In particular, the perfect matchings of the graph are in 1-1 correspondence with the fields of the linear sigma model [10].

4.2.2 Zig-zag paths and the double-line notation

There is one more crucial concept that will be useful in the subsequent discussions. This is the so-called "zig-zag" paths in a dimer model [28, 29]. We define a "zig-zag" path on a graph as follows: starting with some edge on the graph, the zig-zag path starts to the left of the edge and follows parallel to it, then turns to the right and crosses the edge, before turning left so it is parallel to the edge again. Upon reaching a vertex the path turns right and follows parallel to the next edge incident to the vertex, then crosses the edge to the left side and continues parallel, and so on. We demonstrate this in figure 5. We can trace the various arrows and walk a zig-zag path along the edges of the dimer graph.[4]

Such a walk along the edges of the graph indeed traces out a zig-zag pattern. For an arbitrary bipartite graph on T^2, a zig-zag path can intersect itself. But for a dimer model describing a toric gauge theory, it is shown [26, 28, 29] that these zig-zag paths are simple closed curves in T^2 and never intersect themselves. These dimer models belong to a special subclass called "isoradial embeddings" [29].

There is good way to visualize the zig-zag paths using a double-line notation (see figure 5). In this notation, we see that, for our toric dimer models,

[4]The reader may be more familiar with the definition of walking along an edge, such that every time we reach a vertex, we choose to walk to the next vertex which is alternatingly the rightmost and leftmost of the present vertex. Our notation is an equivalent way of representing this.

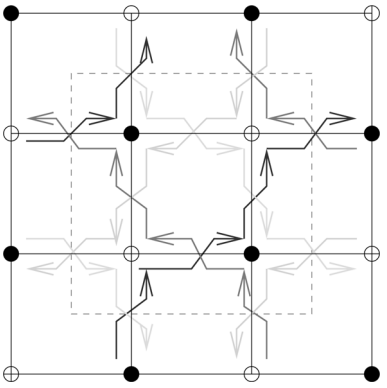

Figure 5: Given a dimer model, we can construct a zig-zag path of alternating leftmost and rightmost directions. A convenient way to represent it is the oriented double-line notation where the zig-zag path crosses an edge at the mid-point. The region inside the dotted line represents a single fundamental domain of the T^2 on which the dimer model is defined.

every edge has two and only two zig-zag paths passing through it with opposite directions. In fact, as we will show later, this double-line notation is not just a convenient tool, but has geometrical and physical meaning.

4.3 From dimer models to planar quivers via (p, q) cycles

It was noted in Equations (2.8) and (2.9) that the intersections of certain (p, q) cycles on T^2 (determined by the slope of external lines in the 5-brane web) count the fields in the quiver. This observation will be given geometrical meaning in Section 7. Here we show that such abstract (p, q) cycles allow one to interpolate between the graph of the dimer model, and its dual graph, the planar quiver.

This is a crucial observation and we summarize it in figure 6. The dimer models are obtained in the limit where the (p, q) cycles form zig-zag paths on an underlying graph. In this limit the zig-zag paths form closed loops around the vertices of the dimer model, with consistent orientation that alternates at adjacent vertices. By consistent we mean that the zig-zag path traces a loop either clockwise or counter-clockwise. This orientation induces the bipartite colouring of the vertices. In the opposite limit the vertices of the dimer model expand to become faces; conversely the faces shrink to vertices, and the edges of the graph become dual edges; thus, we obtain the planar quiver, which is the graph dual. The (p, q) winding cycles allow us to interpolate between the two.

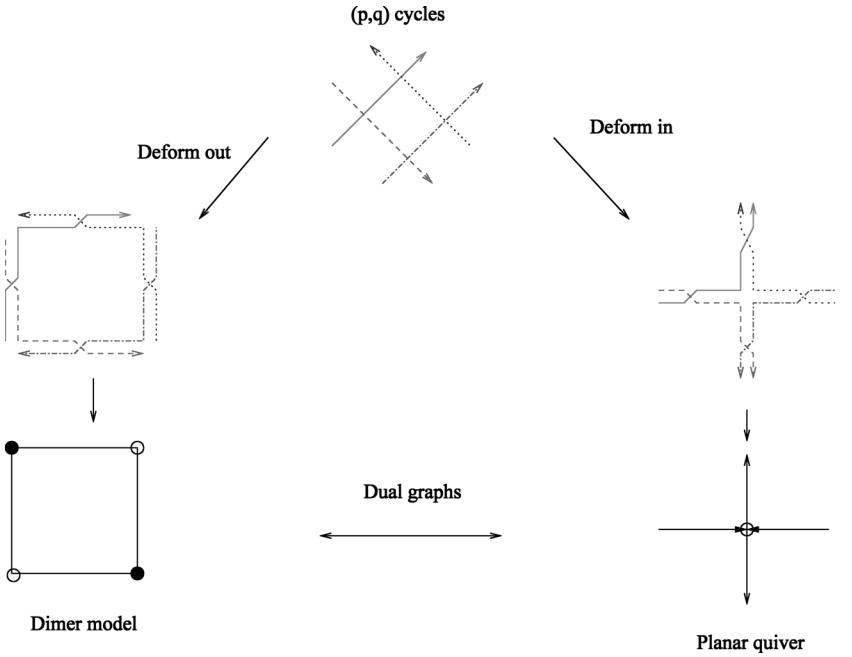

Figure 6: The (p, q) winding cycles on T^2 interpolate between the dimer model and its dual graph, the planar quiver. This crucial observation will be a cornerstone to Section 5.

5 Untwisting the dimer model from T^2 to Σ

Our first task is to identify the dimer model which naturally arises in our construction. We have a dimer model which is related to the gauge theory by simply being the graph dual of the planar quiver. How does this dimer graph relate to our mirror geometry?

In this section we discuss how to isomorphically map between a dimer model on T^2 and a bipartite graph Γ on the curve Σ with the same adjacency matrix. Furthermore, the mapped dimer graph admits an alternative basis of 1-cycles whose intersection properties reproduce the data of the quiver theory, which we may therefore interpret as being part of the locus of the wrapped D6-branes. In fact the D6-branes are obtained by attaching certain discs with boundary along these 1-cycles (together with another S^1 fibre that vanishes along the boundary), as in figure 2. These discs map to the faces of the dimer model on T^2 under the inverse mapping. Together, this will explain the physical relevance of the dimer models to the quiver theories.

The procedure rests on the observation made in Section 4.3 that the dimer model graph may be obtained by taking a limit of intersecting (p, q) winding cycles on T^2, where the polygonal regions enclosed by these cycles with clockwise or counter-clockwise orientations are retracted to produce the bicoloured vertices of the graph. Conversely, given such a bipartite graph, we can "un-glue" it to produce such a set of intersecting (p, q) cycles (the zig-zag paths) by merely reversing this process. Each edge of the dimer model is produced from two such cycles, which cross each other along the edge.

5.1 The untwisting procedure

Given a consistent dimer graph (one whose Kasteleyn determinant defines a convex polygon), the associated zig-zag paths are uniquely determined. In fact, consistency of the zig-zag paths may be used to constrain the allowed dimer graphs (since not every doubly periodic bipartite graph produces a Newton polygon that is convex and therefore defines a toric CY). As illustrative examples, we draw in figure 7 the zig-zag paths associated to the two dimer models describing quiver theories for the CY cone over $\mathbb{P}^1 \times \mathbb{P}^1$, which are related by Seiberg duality [10, 30]. We will have more to say on Seiberg duality later on.

To map the dimer model from T^2 to Σ, recall that each zig-zag path is a winding cycle with (p, q) winding on the T^2 of the dimer model. Furthermore, recall from Section 2.2 (especially figure 3) that each such (p, q) winding cycle is canonically associated to a contour encircling one of the punctures on the curve Σ. The precise sense in which this is true will be discussed in Section 6.1.1, but for now we observe that the (p, q) external legs

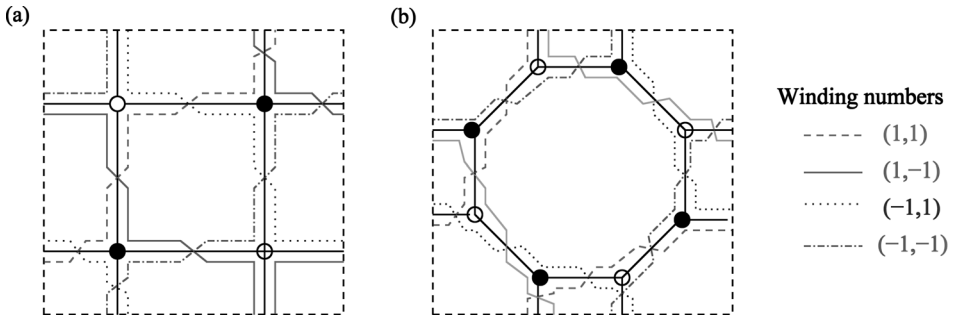

Figure 7: The dimer models for the two Seiberg-dual phases of F_0 are shown in black in (a) and (b), respectively. The zig-zag paths are drawn in colour according to their winding number (direction of paths not indicated explicitly).

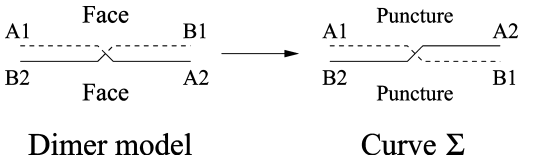

Figure 8: The local untwisting operation that maps the dimer graph to a tiling of Σ. The crossing of two zig-zag paths A, B in the dimer model (left) can be flipped to the boundary of a closed polygon (right).

of the web are mapped to a (p, q) cylindrical region in the neighbourhood of a puncture on the curve.

This suggests that the (p, q) zig-zag path should be associated to an S^1 contour around the corresponding cylinder in Σ. This mapping is realized by a certain "untwisting" operation shown in figure 8. On the left, we show the edge of the dimer model (which separates two faces), given by a crossing of two zig-zag paths. We untwist by flipping this crossing, the zig-zag paths now bound a segment of a closed polygon, whereas the boundary of the dimer model faces (solid and dashed lines) now cross one another. When we later relate these crossing paths to D6-branes, we will obtain a massless chiral multiplet from each crossing.

This is a local operation performed at each crossing of zig-zag paths. It cannot be done as a planar operation on T^2. Indeed, as we will show, it converts a tiling of T^2 to a new tiling of the punctured genus g Riemann surface Σ.

As we successively untwist each edge in the dimer model, the (p, q) winding paths become the boundary of *closed polygons* in the new tiling. These polygons are identified with the cylinders of Σ, so they have a puncture at a point in the interior, and the (p, q) winding paths have mapped to contours encircling the punctures, as anticipated. This procedure amounts to rewriting each zig-zag path on T^2 as the boundary of a new polygon in the plane. Doing this for each zig-zag path, we obtain a collection of such polygons, and when glued together according to the gluing of zig-zag paths on the dimer model, we obtain a tiling of a new Riemann surface. We now show that this new Riemann surface is topologically equivalent to Σ.

Let us demonstrate this in detail, still adhering to the F_0 example above. First, let us re-draw, in figure 9, the zig-zag paths of the two phases (a) and (b) as defined in figure 7; we have now carefully labelled each piece of the zig-zag paths. Now, we can perform the untwisting procedure. The result is given in figure 10. Let us follow, for example, the segments $A7$ to $A8$,

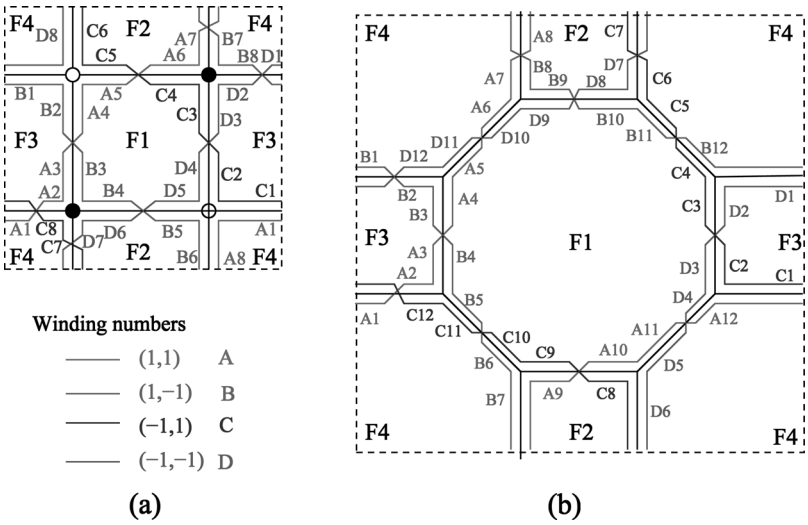

Figure 9: Labelling the path segments on the zig-zag paths. Each segment of the zig-zag paths is glued to another to form the dimer graph in black.

and the juxtaposed $B6$ to $B7$ in figure 9(a). We see that $A7$ and $B7$ are glued together while $B6$ and $A8$ are so glued. Therefore, in figure 10(a), we see that along the boundary of regions A and B, we have the pairs 7–7 and

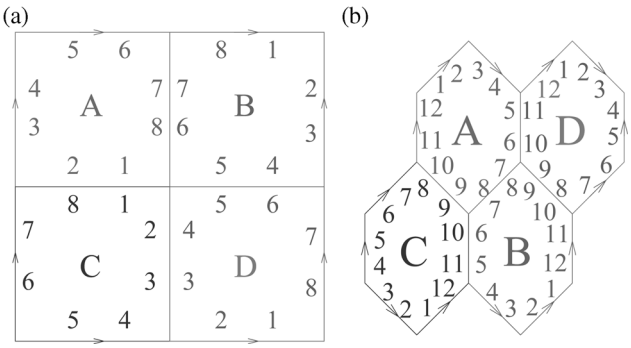

Figure 10: Redrawing the zig-zag paths as bounding polygons in the plane. Since this is a tiling of a genus 1 curve, opposite sides in the tiling are to be identified. From the two dimer models of F_0 shown in figure 9, we obtain two tilings of a genus 1 curve with a puncture in the interior of each of the four faces, which we identify with the curve $P(z, w) = 0$. The two Seiberg-dual dimer models correspond to two different choices of gluing. Note that the quartic and trivalent vertices of the dimer model are preserved in this tiling of Σ by construction, so strings may interact locally around such a vertex to produce superpotential terms.

8–6 being adjacent. So too, are, for example, $C2$–$D4$ and $C3$–$D3$, etc. In this picture, the zig-zag paths are simply the boundaries of the polygonal regions A, B, C, D, which correspond to the punctures in Σ.

Now let us discuss the genus of the surface which results from this gluing. Recall, for the dimer model on T^2 we had, from (4.3),

$$V + N_g - N_f = 2 - 2 \times 1 = 0 \tag{5.1}$$

where V are the vertices of the dimer model, N_g the number of faces (which correspond to gauge groups of the quiver theory), and N_f the number of edges of the dimer model (fields in the quiver theory).

Each puncture on the curve $P(z, w) = 0$ comes from a semi-infinite external line in the (p, q) web, equivalently to a line segment on the boundary of the toric diagram. The number N_p of such segments is equal to the number of lattice points on the boundary on the toric diagram (what we called external points). The number of gauge groups in the quiver theory is equal to twice the area of the toric diagram, which by Pick's theorem [31] (see, e.g., [29] in this context) is given by

$$N_g = 2\,\text{Area} = 2I + N_p - 2 \tag{5.2}$$

where I is the number of internal points. Thus,

$$V + N_p - N_f = 2 - 2I. \tag{5.3}$$

Therefore, the result of the untwisting is a Riemann surface of genus $g = I$. Now, the vigilant reader would recall the fact from (2.5) that the genus of a curve is equal to the number of internal points of its Newton polygon. Hence, we have reconstructed the surface Σ, of genus I. Indeed, the faces of this polygonal tiling are in 1-1 correspondence with the punctures of Σ, as desired.

The above construction amounts to giving a double meaning to each (p, q) zig-zag path: *it is the* (p, q) *winding cycle in the* T^2 *of the dimer model; it is also the boundary of a face in the tiling of the curve* Σ*, associated to a punctured region.*

Indeed, there is another set of 1-cycles constructed from the combination of various segments of zig-zag paths. For example, in (a) of figure 9, we can take the closed loop formed by $A4$–$A5$–$C4$–$C3$–$D4$–$D5$–$B4$–$B3$. Such cycles bound each face using the dimer model, which was associated to a gauge group in the dimer model rules. After untwisting to construct the surface Σ, one may trace these paths in the tiling of Σ and verify that they generically turn into 1-cycles with non-trivial homology class.

What we have done is to start with a dimer model which tiles T^2 (and whose dual graph is the planar quiver) and simply re-identified the faces and edges using the untwisting procedure. The result is a new bipartite graph Γ, i.e., a new dimer model, which now tiles the Riemann surface Σ of genus $g = I$.

5.1.1 Summary: duality between dimer models on T^2 and $\Gamma \subset \Sigma$

In summary, we find a kind of duality between dimer models in T^2 and the new bipartite graph Γ in Σ: *the winding cycles and boundary of faces of one object are mapped to the boundary of faces and the winding cycles of the other.*[5]

In fact, it is clear that apart from re-identifying the nature of the faces of the dimer graph, (i.e., considered as an operation on the abstract graph itself), the twisting operation is a *graph isomorphism* since we do not change the adjacency of the edges or the vertices. In particular, the dimer model on Γ is the same as the dimer model on its twisting[6] to T^2.

Note that this construction is not limited to the case where Σ has genus 1 as in [4]. For $g > 1$ the wrapped branes correspond to some combination of the A_i and B_j cycles of the curve, and one may use the zig-zag construction to read off their homology class and intersection numbers.

By construction, we have not changed any of the data of the quiver theory, which was efficiently packaged in the graph of the dimer model. We have simply redrawn the graph of the dimer model as a certain graph on the curve $P(z, w) = 0$, with the same combinatorial properties. This graph winds the non-trivial cycles of Σ, and certain of these cycles are those wrapped by the D6-branes, which we will discuss further in the next section.

For now, let us present 2 illustrative examples. In figure 11, we study the $\mathbb{C}^3$ geometry encountered in figure 4. Here, Σ has $g = 0$, and is a 3-punctured sphere. The dimer model was drawn in figure 4 and has a single face. The face is dualized to a single bounding path on the sphere.

In figure 12 we study the conifold. For completeness, we also included the toric diagram, the quiver (as well as the periodic planar quiver) diagrams

[5]This duality was called the *antimap* in [32]. We thank D. Vegh for pointing out this reference to us.

[6]It is interesting to note that since these two dimer models are isomorphic, they have the same characteristic polynomial, and we have produced a dimer model that is *defined on its own spectral curve* $\det K = 0$.

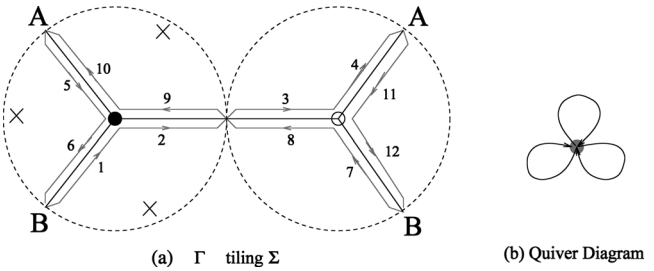

Figure 11: (a) The graph Γ obtained by untwisting the dimer model for $\mathbb{C}^3$ (see figure 4). The curve Σ is obtained by gluing the two discs back-to-back along their boundary circle so that the points A, B coincide. The three punctures on the curve correspond to the faces of the graph Γ. The single face of the dimer model maps to a single self-intersecting contour (path segments numbered sequentially) that produces the correct quiver for the world-volume theory (shown in (b)). Moreover, the two trivalent vertices of Γ produce the cubic superpotential.

and the dimer models of the theory. The Riemann surface Σ is here again of genus 0, now with 4 punctures. We have labelled the 4 fields $p_{1,2}, q_{1,2}$ explicitly in part (a). Upon graph-dualizing to the dimer model in (b) the fields become edges and we retain their naming while the + (resp. −) face becomes the white (resp. black) node.

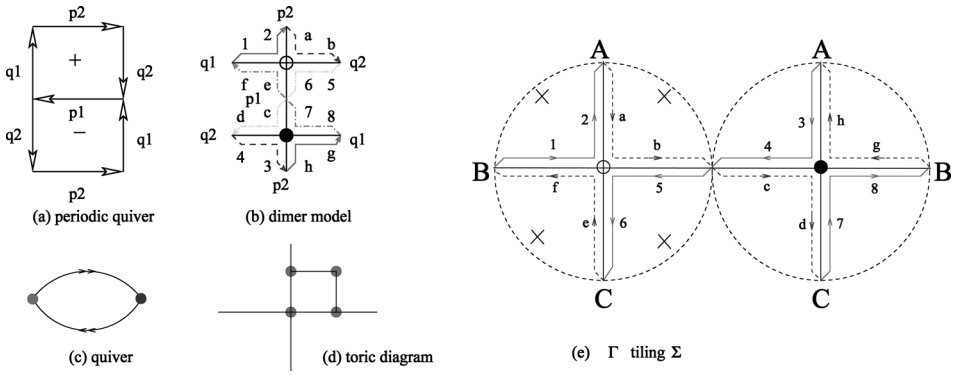

Figure 12: The graph Γ obtained by untwisting the dimer model for the conifold in shown in (e). For reference, we also draw the quivers, the dimer model and the toric diagram. The two faces of the dimer model produce two intersecting contours on Σ, whose intersections produce the quiver diagram for this theory. The two quartic vertices of Γ give rise to the quartic superpotential of the quiver theory.

5.2 The gluing locus

We have seen how dimer models on T^2 can be untwisted to give dimer models on Σ (and vice versa). In light of the discussions in figure 2 and Section 3, we see that all this takes place as we glue Σ from its semi-infinite cylinders (punctures). The untwisting procedure thus furthermore provides a decomposition of Σ into half-infinite cylinders. We show this in figure 13 for our familiar $\mathbb{C}^3$ example.

What about the converse operation to this decomposition? As discussed in the previous subsection, for each puncture on the curve, we obtain a half-infinite cylinder. The curve $P(z, w) = 0$ may be recovered by gluing together the set of deformed cylinders along their S^1 boundaries. The gluing locus corresponds to a graph Γ inscribed on the curve Σ, as shown in figure 13. Said differently, we take contours that encircle the punctures of Σ and evolve them continuously into the interior until they meet. When they join up completely they do so along the graph Γ.

The various Seiberg-dual phases of the quiver theory are among the possible graphs obtained by such gluing. However, not every such Γ describes a consistent dimer model (Γ may not even be bipartite, although it may always be possible to obtain it as the limit of a bipartite graph when some edges shrink to zero). Even for bipartite graphs, the zig-zag paths on this graph may not produce a consistent quiver theory (similarly, neither does every dimer model on T^2). We leave this problem for future study.

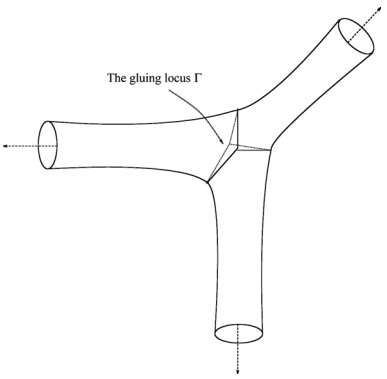

Figure 13: Gluing together three half-infinite cylinders along their S^1 boundaries to form the curve $1 + w + z = 0$, which is part of the mirror to $\mathbb{C}^3$. The gluing locus is as shown in figure 11.

5.3 Dimer models from mirror symmetry

We are now able to combine the discussion of the previous sections to show how the intersecting D6-branes are equivalent to the dimer models on T^2. As discussed in Section 2.1, each D6-brane is associated to a disc that is stretched from the vanishing cycle in the fibre above a critical point in the W-plane, to the fibre above $W = 0$, i.e., the boundary of the disc is attached along an S^1 in the curve Σ, see figure 2.

In the previous section we showed that the various S^1s form zig-zag paths on a certain graph Γ inscribed in this curve. Γ defines a tiling of Σ. The faces of this tiling correspond to the punctures on Σ (i.e., the half-cylinders), and the winding cycles (zig-zag paths) on this curve are the D6-branes.

The intersection of these D6-branes with each other produces the matter content of the quiver (including any non-chiral matter): since the zig-zag paths cross along every edge, in string theory we obtain a massless chiral multiplet localized at the intersection point, coming from the massless stretched string with consistent orientation [33].

Furthermore, the vertices of Γ, where multiple zig-zag paths form a closed loop around the vertex, give rise to the superpotential terms. These are computed by world-sheet disc instantons ending on this loop.

The discs associated to the D6-branes intersect to form a T^2 embedded in the mirror geometry. To visualize the T^2 one may use the twisting operation described in the previous section. After twisting the graph Γ, we have a tiling of T^2, the dimer model. The S^1 winding paths on Γ map to the boundary of the faces of the tiling, and the discs attached along these S^1 map to the interior of the faces. The vertices of Γ *remain* vertices of the dimer model on T^2.

This explains the origin of the dimer models on T^2 and their relevance for describing the physics of the quiver gauge theory. It also explains the physical relevance of the observation (2.9) about the number of fields of the quiver being counted by the intersection of (p, q) winding cycles on a T^2, since we obtain such cycles by twisting the D6-branes from Σ to T^2.

In general, the T^2 of the dimer model together with the intersection along the curve Σ can only be embedded in 4 dimensions, since in 3 dimensions the discs attached along the S^1s would have to pass through one another. This is indeed the case here, since the curve Σ is defined in $(\mathbb{C}^*)^2$. Furthermore, we claim that the twisting operation discussed in the previous section may be performed *continuously* when the system is embedded in the

mirror geometry. This identifies the T^2 of the dimer model with a $T^2 \subset T^3$ of the world-volume of the D6-branes. The remaining S^1 fibre is given by phase rotations in the uv-plane, which is finite over the interior of the faces (away from $W = 0$), and vanishes along the graph of the dimer model (above $W = 0$). This gives a singular T^3, which is identified with the mirror to the D3-brane at the singular point. Thus, we have obtained a concrete construction of the dimer models using mirror symmetry.

We can now clarify the status of the NS5-D5 "brane tilings" proposed in [10] (see also [34]), at least heuristically. If we T-dualize along the S^1 fibre in the uv-plane, we should obtain an NS5-brane at the point where the fibre becomes singular, i.e., above $W = 0$. Thus, the NS5-brane will wrap the curve Σ. Since the D6-branes were extended along this fibre direction, they become D5-branes with topology of a disc, with the boundaries of these discs intersecting along the $NS5$-brane. Together these D5-branes form a T^2 embedded in the geometry, and the graph of the dimer model is again the locus where the T^2 intersects the curve wrapped by the NS5-brane.

Therefore, one may indeed hope to obtain the dimer model from an intersecting NS5-D5 system, although it is difficult to be clear about the geometry of this system since it is not prescribed directly by local mirror symmetry. In particular it clarifies the relation of the T^2 of the dimer model to the geometry of the NS5-brane, which turns out to have been not quite correctly specified in previous literature.

5.4 Seiberg duality

Now we discuss how to understand Seiberg duality in our picture. Again we illustrate with the above F_0 example. In figure 14, we have redrawn the two phases presented in figure 9, but now as a dimer model in Σ. Here, we have used L_i to denote the boundary to be glued together by our lifting procedure. The first thing we need to notice is that while the gluing of the left figure is a straight-forward rectangular one, the gluing of the right figure has some shifting. That is, these two figures have different complex moduli-parameters τ of the resulting Σ, which here happens to be a (punctured) torus.

The second thing we need to notice is that, as we have discussed before, the boundary of faces in the dimer model lifts to non-trivial cycles in Γ. Here we have redrawn these liftings carefully and recorded their non-trivial homology classes in Γ. We have written down these (p, q)-cycles in Σ in the

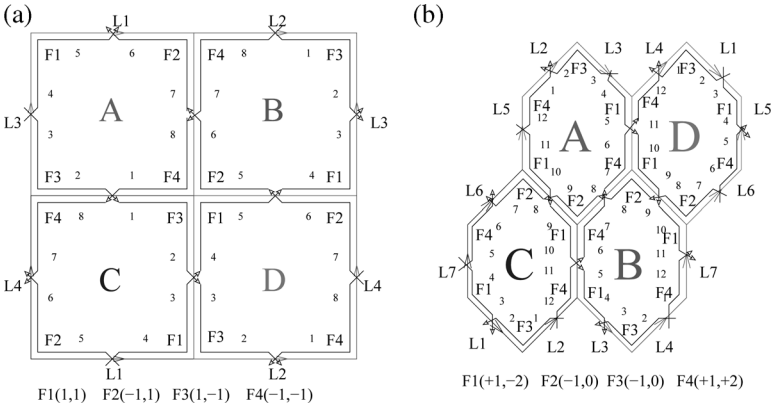

Figure 14: The two Seiberg dual phases of F_0 from (9), here drawn as dimer model in Σ using the twisting procedure. We have labelled the segments and direction of the zig-zag paths explicitly.

figure. They are

$$\begin{array}{ll} (a)(F_0)_{II} & F1(1,1),\ F2(-1,1),\ F3(1,-1),\ F4(-1,-1) \\ (b)(F_0)_I & F1(1,2),\ F2(-1,0),\ F3(-1,0),\ F4(1,-2). \end{array} \tag{5.4}$$

It is easy to check that the intersection number given by $\chi(i,j) = \det \begin{pmatrix} p_i & q_i \\ p_j & q_j \end{pmatrix}$, which we recall from (2.8), gives the right matter contents for both phases.

In fact these two different sets of cycles have been observed in [35] on the discussion of the relation between the (p,q)-web and quiver theory. Such a relation has been clarified further in [36] where two different terminologies, viz., the toric (p,q)-web and the quiver (p,q)-web, have been distinguished. Now, from our construction, it is clear that the toric (p,q)-web corresponds to zig-zag paths on T^2 while the quiver (p,q)-web corresponds to cycles in Σ. The latter, of course, only makes sense if Σ were a torus as well, which only happens if there is one internal point in the toric diagram. Indeed, as we have emphasized, in general Σ can be of arbitrary genus. In this case, a single pair of (p,q)-charges (corresponding to the quiver (p,q)-web) no longer makes sense. However, it still has meaning in the dimer model on T^2.

Now, we would like to show that these two sets of cycles in (5.4) are related to each other by Picard–Lefschetz (PL) transformations, which we recall from [4] and [17]. Let us start from the set

$$F3(1,-1) \quad F1(1,1) \quad F2(-1,1) \quad F4(-1,-1), \tag{5.5}$$

where we have reordered these cycles cyclically according the rules in [17]. Now we move $F1$ to the right of $F2$. The new cycle of $F2$ is given by $(-1,1)+\chi(1,2)(1,1)=(1,3)$. However, since the new $n_{F1}=1-\chi(1,2)=-1$ we need to add extra sign for the charge of $F1$. In other words, we have new cycles:

$$F3(1,-1) \quad \widetilde{F2}(1,3) \quad \widetilde{F1}(-1,-1) \quad F4(-1,-1). \tag{5.6}$$

It is then easy to check that (5.6), when acted upon by an $\mathrm{SL}(2,Z)$ transformation $\begin{pmatrix} 1 & 0 \\ -1 & 1 \end{pmatrix}$, gives us:

$$F3(1,-2) \quad \widetilde{F2}(1,2) \quad \widetilde{F1}(-1,0) \quad F4(-1,0). \tag{5.7}$$

This we instantly recognize to be the set (b) (up to cyclic permutation). We conclude, that the sets (a) and (b), obtained from our two different gluings, indeed are PL dual, and, hence, Seiberg dual, to each other. It is for this reason that we have judiciously labelled in (5.4), the two phases as $(F_0)_I$ and $(F_0)_{II}$, in the convention of the literature (cf. e.g., [37]).

5.5 Summary of the various correspondences

We have introduced many concepts in this section, so before proceeding to the next section where we will see how in some cases one may concretely realize the T^2 in the geometry, we find it expedient to summarize some key results discussed above by itemizing the correspondences amongst the various objects:

- The (p,q)-web is the graph dual of the toric diagram D of $\mathcal{M}$, while the dimer model on T^2 is the graph dual of the quiver diagram, when drawn as a planar graph on T^2.
- The mirror geometry $\mathcal{W}$ of $\mathcal{M}$ is given by a double fibration over a W-plane, consisting of a $\mathbb{C}^*$ fibre ($uv=W$) and a (punctured) Riemann surface Σ defined by $P(z,w)=W$. The expression $P(z,w)$ is the Newton polynomial $P(z,w)$ of D (cf. figure 1 and equation (2.2)). The genus of Σ is equal to the number of internal points of D. Moreover, Σ is a thickening of the (p,q)-web, while its punctures, which tend to cylinders at infinity, are aligned with the (p,q)-legs (cf. figure 3).
- The (p,q) winding cycles on a T^2 can be deformed into zig-zag paths on the dimer model on T^2, or, dualistically, to a bounding of the

planar quiver (cf. figure 6). The direction (clock-wise or counter-clockwise) of the loops formed by the zig-zag paths around each vertex of the dimer model gives the bipartite nature of the dimer model (cf. figure 5).

- The dimer model on T^2 can be mapped, using an untwisting procedure, to an isomorphic bipartite graph Γ on the curve Σ, which is part of the mirror geometry. In particular, a zig-zag path with (p, q) winding maps to an S^1 that winds around the puncture along the (p, q) direction in Σ (cf. figures 11, 12). Conversely, we can glue cylinders to form Σ; then, the S^1 winding the punctures (cylinders) join along Γ (cf. figure 13).
- Dualistically, a closed loop formed by segments of different zig-zag paths, whereby bounding a face in the dimer model (cf. figure 9), lifts to a winding path around a non-trivial homology cycle in Σ and forms a zig-zag path on Γ.
- The zig-zag paths on Γ are the intersection of the D6-branes with Σ; their intersection with one another on Σ dictates the quiver theory. Thus, #(faces of dimer model) = #(gauge groups in quiver) = #(critical points of $P(z, w)$) = #(non-trivial 3-cycles in $\mathcal{W}$) = 2 Area(D). Vertices of Γ give superpotential terms via string world-sheet disc instantons bounded by the parts of the D6-branes that combine to form a loop around this vertex.
- These intersecting D6-branes span a singular T^3 according to mirror symmetry, and there is a distinguished T^2, which is the complement of the S^1 (defined by $uv = 0$) that vanishes at $P(z, w) = 0$. This is the T^2 on which the dimer model is defined. The S^1 fibre vanishes along the graph of the dimer model, which is where the D6-branes (and the T^2) intersects Σ defined by the curve $P(z, w) = 0$. The twisting map is a convenient way to map the T^2 spanned by the D6-branes in the mirror geometry to an abstract T^2, in order to visualize this dimer model. Below, we will see another concrete way to visualize this T^2.

6 Amoebæ and algæ

In the previous sections we discussed a topological map that allowed us to go between the dimer models on T^2 and the intersection locus of the D6-branes on the curve $\Sigma \subset (\mathbb{C}^*)^2$. We now discuss how one may also obtain this T^2 from a certain projection of the geometry. This is the concrete realization mentioned in Section 3. This projection is a counterpart of the so-called amoeba projection used in algebraic geometry, which we now review.

6.1 The amoeba map

Let us parametrize the coördinates $(z, w) \in (\mathbb{C}^*)^2$ as

$$(z, w) = (\exp(s + \imath\theta), \exp(t + \imath\phi)) \tag{6.1}$$

where $s, t \in \mathbb{R}$ while $\theta, \phi \in [0, 2\pi)$. Thus, the space $(\mathbb{C}^*)^2$ has topology $\mathbb{R}^2 \times T^2$. It is difficult to visualize this 4-dimensional space directly, however two projections will be of vital importance. The first is the projection of the curve onto $\mathbb{R}^2$:

$$(\exp(s + \imath\theta), \exp(t + \imath\phi)) \mapsto (s, t) \tag{6.2}$$

This projection is known in the literature as the *amoeba* of the curve, because the resulting shape of the projected curve is reminiscent of the mischievous microbe (see figure 15(a)).

Let us discuss the projection (6.2) in detail first. The reader is referred to [21, 25, 38–40]. The formal definition applies to any variety. Let $V \subset (\mathbb{C}^*)^n$ be an algebraic variety and let

$$\text{Log} : (\mathbb{C}^*)^n \to \mathbb{R}^n \text{ be the map } \text{Log}(z_1, \ldots, z_n) \to (\log|z_1|, \ldots, \log|z_n|) \tag{6.3}$$

for coördinates $z_{1,\ldots,n}$ of $(\mathbb{C}^*)^n$. Then the amoeba of V is a real algebraic set

$$\text{Amoeba}(V) := A = \text{Log}(V) \subset \mathbb{R}^n. \tag{6.4}$$

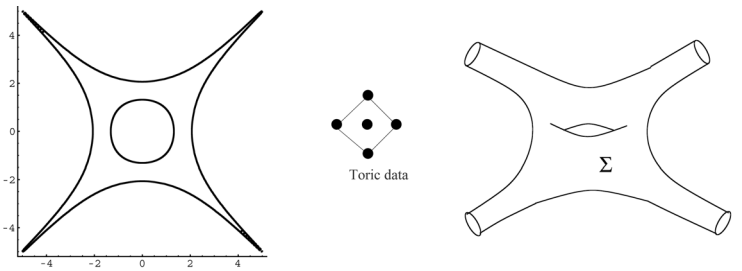

(a) Boundary of Amoeba (b) Toric Diagram and Riemann Surface

Figure 15: The amoeba of the Riemann surface $P(z, w) = -w - z - 1/w - 1/z - 6$, which corresponds to the zeroth Hirzebruch surface introduced in figure 3 in drawn in (a) and the boundary, in (b). The amoeba has tentacles which asymptote to lines which are called spines, which is the dual graph to the toric diagram, i.e., the (p, q)-web. For reference we include the toric diagram and the Riemann surface Σ in (c).

Our focus is on the curve $P_W(z, w) = 0$ and the amoebae will be regions in the plane $\mathbb{R}^2$. The map (6.3) is, of course, the same as the projection (6.2) stated above.

6.1.1 Amoebæ and the (p, q)-web

One of the first attractive qualities of the amoeba, as one can see from figure 15(a), is its *tentacles* which extend exponentially to infinity, asymptoting to a straight line. Such a line is called a *spine* of the amoeba. We can determine the directions of these spines readily and will show the important fact that they are simply given by orthogonal directions of the external edges in the toric diagram. That is, the tentacles line up with the dual graph to the toric diagram.

Using an $\mathrm{SL}(2, \mathbb{Z})$ transformation plus a shift we can always rotate the toric diagram so that the Newton polynomial is given by

$$P(z, w) = \sum_{i=0}^{n} c_i z^i + wG(z, w)$$

with $G(z, w)$ a polynomial of z, w with only non-negative powers. The number $(n + 1)$ is the total number of lattice points along the external line that is now aligned with the z-axis. The limit $w \to 0$, i.e., as $\log |w| \to -\infty$, we have the tentacles tending to negative vertical direction.

Rewrite $P(z, w) = 0$ as

$$\sum_{i=0}^{n} c_i z^i = c_n \prod_{i=1}^{n} (z - z_i) = -wG(z, w),$$

where we have factorized the polynomial in z into its roots z_i. Therefore, as $w \to 0$, we have that $\prod_{i=1}^{n}(z - z_i) \to 0$ and we get n asymptotes along the vertical negative (i.e., $\log |w|$) direction located at positions $\log |z_i|$. In other words, we have that the asymptotic spines are orthogonal directions to (i.e., dual graph of) the toric diagram. Recalling from the above discussions in Section 2.2, that this dual graph is precisely the (p, q)-web, we conclude and summarize[7]

> *The spine of the amoeba of $P(z, w)$ is the (p, q)-web associated to the toric diagram which is the Newton polygon of $P(z, w)$.* Conversely, the amoeba is a thickening of the (p, q)-web.

[7] In the mathematics literature (cf. e.g., [40]), the spine is considered a deformation retract of the amoeba and one usually shows this fact using the points of non-differentiability of a so-called Ronkin function.

The origin of these deformations from the (p, q)-web to the curve Σ are the torus-invariant world-sheet instantons, which localize near the trivalent vertices of the (p, q) web (T^3-invariant points) prior to performing mirror symmetry (recall from Section 2.2 that the web describes a $T^2 \times \mathbb{R}$ special Lagrangian fibration of the geometry). Mirror symmetry amounts to summing these instanton corrections, and produces the effective geometry described by the local mirror.

The above observation gives another interesting result. Notice that for general moduli c_i, the tentacles are parallel along different locations $\log|z_i|$. However, if some of $\log|z_i|$ are the same, then the corresponding tentacles will merge. The most degenerate case is if all the $\log|z_i|$ are same. In this case, we have one and only one tentacle. Furthermore, if we assume that all z_i are real and positive, as was needed in [9] to compare with the linear-sigma model, we immediately have that

$$(z-a)^n = a^n(z'-1)^n = a^n \sum_{k=0}^{n} (-1)^k \frac{n!}{k!(n-k)!} z'^n,$$

where $z' = z/a$. We see that the coefficients $\frac{n!}{k!(n-k)!}$ are nothing but the linear sigma model field multiplicities conjectured in [37], for the case of colinear points on the boundary of the toric diagram.

6.1.2 Amoebæ and dimer models

Not only are amoebæ related to (p, q)-webs, they have appeared in relation to dimer models in previous work [25, 26]. For our purposes one especially pertinent issue is that of *Harnack curves*.

Harnack curves date back to Hilbert's 16th Problem concerning the possible topologies of degree d real algebraic curves C in $\mathbb{RP}^2$. Harnack proved [41] that the number of components of C can not exceed $\frac{(d-1)(d-2)}{2} + 1$ and when this maximum is attained, C is now known as a *Harnack curve*. These are in some sense the "best" or most generic real curves. Recalling the definition of the spectral curve an edge weights of a dimer model, a main result of [25] is that

> *For any choice of real edge weights subject to a certain sign constraint, the spectral curve of a dimer model is a Harnack curve.*

Harnack curves have very nice amoeba projections, in particular, their amoebæ can be analytically described by a single inequality (with the

boundary satisfying the equality):

$$P_W(z,w) \text{ Harnack } \Rightarrow \text{Amoeba}(P_W(z,w)) = \left\{ (x,y) \in \mathbb{R}^2 : \prod_{\alpha,\beta=\pm 1} P_W(\alpha e^x, \beta e^y) \leq 0 \right\}. \quad (6.5)$$

In this paper, we shall however relax the constraint of reality on the coefficients in $P_W(z,w)$ and hence will not deal much with Harnack curves, or, for that matter, real curves. This means that in the dimer models we relax the constraint on the signs and reality of edge weights. This turn out to be necessary for the dimer model to explore the full moduli space of the Calabi–Yau geometry (cf. A. Craw, R. Karp and K. Kennaway, Work in progress.). The price is that even though the Kasteleyn determinant is still a sum over perfect matchings of the graph, they are no longer counted with uniform sign. As we learned from [9], the Harnack nature of the spectral curve was good for combinatorics and unveiled the nature of GLSM field multiplicities, but for now this is not relevant for us. We can still recover the special Harnack case if we choose edge weights to satisfy appropriate constraints.

6.2 The alga map

The map (6.2), which leads to the amoebæ and has been widely studied by mathematicians, is but one of 2 natural projections. Whereas (6.2) projected onto the real parts of $(z,w) \in (\mathbb{C}^*)^2$, we now project to the imaginary (angular) part:

$$(\exp(s+\imath\theta), \exp(t+\imath\phi)) \mapsto (\theta, \phi). \quad (6.6)$$

This is a projection onto a T^2 component of $(\mathbb{C}^*)^2$ and by projecting every point on the curve $P_W(z,w)$ to its angular component, we obtain a doubly periodic image of the curve. In keeping with the microbial naming convention, we call these doubly periodic projections *algae* of the curves, after the microscopic plant species which like to tile surfaces in bodies of water. We illustrate this with an example in figure 16. We will show below that the T^2 of the dimer models can be identified with the above T^2 inhabited by the algae, at least in certain cases.

As far as we are aware, the properties of this projection have not been studied by mathematicians. For the amoeba map, the boundary may be parametrized explicitly when the curve is Harnack (see (6.5)). In this case, the curve admits the antiholomorphic involution $(z,w) \mapsto (\overline{z}, \overline{w})$. This fixes

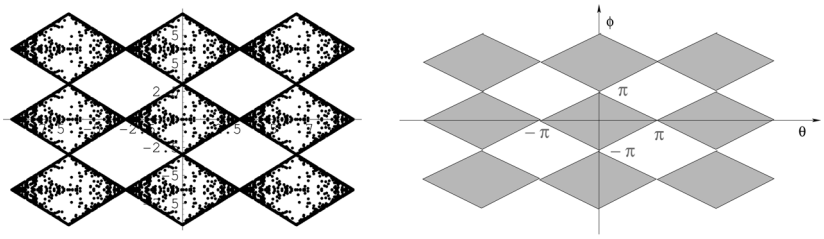

(a) (b)

Figure 16: (*a*) The alga of F_0 (cf. figure 15) draw using Monte–Carlo and redrawn in (*b*) to show the boundaries more clearly. We have indicated 3×3 of the fundamental region to show the periodicity. Not all algæ are as regular as this.

the boundary, and shows that the curve is 2-1 over the interior of the amoeba, with those points related by complex conjugation.

Therefore, under the alga projection the boundary of a Harnack curve maps to the points $(0,0), (0,\pi), (\pi,0), (\pi,\pi)$ since it is real. The rest of the alga is symmetric under the map $(\theta,\phi) \mapsto (-\theta,-\phi)$ which descends from the involution on Σ. Beyond this, we do not know how to explicitly parametrize the alga projection, let alone in the non-Harnack case. In practice, we therefore resort to Monte–Carlo simulation to plot its interior. Furthermore, as we discuss later, to get a non-degenerate alga projection of the dimer models we really need generic complex moduli in the curve $P(z,w)$.

7 Dimer models from algæ

In this section we describe how the graph of the dimer models may be obtained by the alga projection of the intersecting D6-brane system discussed in Section 5.3.

Recall that the dimer models on T^2 may be obtained by "twisting" the intersection locus of the D6-branes with the curve $P(z,w) = 0$. Key to this twisting procedure was the fact that the graph Γ on which the D6-branes are zig-zag paths admits a decomposition into contours encircling the (p,q) spines of the curve Σ. After the twisting map these became the (p,q) winding cycles of the torus.

We will now show that the same is true when we project onto the T^2 defined by the alga projection, and furthermore that in certain situations the T^2 obtained by twisting may be identified with the projection onto the angular variables.

7.1 The (p, q) winding cycles

Recall from our above discussions in Section 6.1.1 that the spine of the amoeba aligns with the (p, q)-web. In particular, consider the simple case where we have only 2 lattice points for a given external edge in the toric diagram whose normal direction is (p, q). Then we can normalize P to the form

$$P(z, w) = c_1 + c_2 z^{-q} w^p + \sum_i c_i z^{-q_i} w^{p_i}. \tag{7.1}$$

Rescaling $z \mapsto \lambda^p z$, $w \mapsto \lambda^q w$, the curve becomes

$$P(z, w) = \frac{c_1}{c_2} + z^{-q} w^p + \sum_i \frac{c_i}{c_2} \lambda^{(p,q)\cdot(-q_i,p_i)} z^{-q_i} w^{p_i} = 0. \tag{7.2}$$

Since the toric diagram is convex, in the limit $\lambda \to \infty$ only the first two terms survive, and the curve becomes

$$P(z, w) = z^{-q} w^p + \frac{c_1}{c_2} = 0, \tag{7.3}$$

i.e., in the neighbourhood of a puncture of $P(z, w) = 0$, the curve approaches a flat cylinder

$$z^{-q} w^p = -\frac{c_1}{c_2}. \tag{7.4}$$

The constant is given by the ratio of the coefficients of the two vertices forming the edge of the Newton polygon that is orthogonal to the (p, q) spine.

This cylinder admits the $\mathbb{C}^*$ action

$$z \mapsto \lambda^p z, \quad w \mapsto \lambda^q w \tag{7.5}$$

and so the cylinder is described by a trivial S^1 fibration over a line. Under the projection to the alga, this S^1 maps to a straight line with (p, q) winding and with offset given by $\arg(-c_1/c_2)$, i.e., determined by two of the moduli of the curve. In other words, (7.4) projects to

$$q\theta - p\phi = \arg(-c_1/c_2) \tag{7.6}$$

which is a straight line with winding number (p, q) in the T^2 defined by the alga projection. On the other hand, the base of the fibration is the spine and is a line aligned in the (p, q) direction in $\mathbb{R}^2$ under the amoeba projection. Thus, *just as the amoeba can be viewed as a thickening of the (p, q) web whose semi-infinite legs (spines) are straight lines of slope (p, q), so too can the alga be viewed as a thickening of the straight line winding cycles with slope (or winding number) (p, q).*

The above observations are for S^1 cycles far away along the spines. Now if we deform these contours, the projection to the alga will also deform.

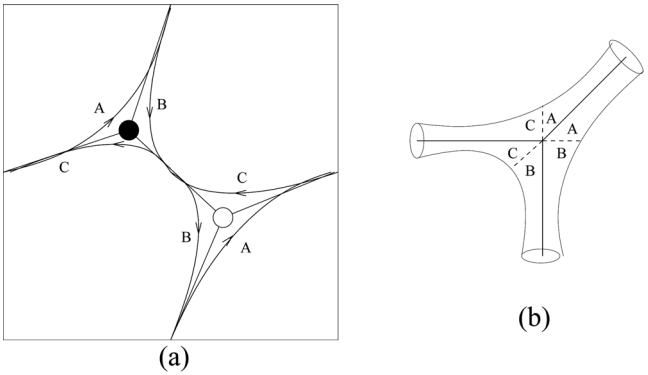

Figure 17: (*a*) The projection of the gluing locus for $\mathbb{C}^3$ onto the alga. The three punctures on the curve define cylinders along the $(1,1)$, $(0,-1)$ and $(-1,0)$ directions which project to cycles with the same winding number, labelled by A, B and C. They are shown as smooth curves, and in the limit where they glue together they meet along the locus in blue, which is the graph of the dimer model for $\mathbb{C}^3$. Note that the bipartite nature of the graph follows automatically, since neighbouring vertices are surrounded by opposite orientations. This choice of (p,q) winding cycles bound polygonal regions on the torus, which are the faces of the dimer model and will later be identified with the wrapped branes. Note that each "edge" of the faces is produced by two intersecting (p,q) cycles, which will each give rise to a bifundamental chiral multiplet. (*b*) The dashed lines on the curve $P(z,w)=0$ shows the gluing locus, i.e., the graph Γ.

Suppose that there exists a family of contours encircling the punctures on Σ such that under the projection to T^2 the boundary of the n-valent polygons (i.e., polygons bounded by consistent orientation) retracts onto n-valent vertices in the interior, as shown in figure 17. Then one obtains a doubly periodic bipartite graph in the T^2, which is a dimer model for the quiver theory. One recognizes the retraction of the straight-line paths as the zig-zag paths introduced in figure 5.

This points towards the geometrical origin of the dimer models as winding cycles on the curve $P(z,w)=0$. However, it is not the end of the story, because in string theory we obtain the massless matter of the quiver theory from the intersection of D6-branes, so we must choose a set of contours that intersect with the correct properties. Clearly, the straight-line contours do not satisfy this, since they do not intersect one another on Σ because they are far away along the spines.

However, we saw in Section 5 that there indeed exists a suitable deformation of these contours on Σ to produce the dimer model as above, namely

the graph Γ introduced therein. It may be constructed by suitably gluing together a set of contours that encircle each of the punctures on the curve. We constructed this graph using the untwisting map from the dimer models on T^2, and observed that the resulting graph has the correct properties to support the wrapped D6-branes that produce the desired quiver gauge theory on their world-volume.

Given a suitable embedding of this graph $\Gamma \subset \Sigma$, which was obtained by a map from an *abstract* T^2, we will show that the graph of the dimer model is again reproduced by projecting to the *particular* T^2 defined by the angular parts of (z, w), and argue that these T^2 may be identified in such cases. However, it is important to keep in mind that the image in this alga T^2 is a projection of the curve in which we have discarded half of the information (by projecting onto a half-dimensional subspace of $(\mathbb{C}^*)^2$). It may sometimes be the case that the projection to the T^2 is not faithful, e.g., contours that cross after the T^2 projection may not really cross on the curve Σ. It is therefore better in general to consider the contours on Σ rather than their projection; we discuss this further in Section 7.5.

7.2 Projection of the intersection locus

If we assume that the embedding of the graph Γ is such that the projection to the T^2 is an isomorphism (i.e., there do *not* exist two distinct points on Γ with the same angular parts), then the alga projection of Γ is identified with the graph of the dimer model obtained by the twisting procedure of Section 5, up to homotopy. We conjecture that it is always possible to arrange this, and we give several examples in Section 7.4.

Even in non-degenerate cases, identifying the T^2 of the dimer model with that of the angular variables imposes additional restrictions on the properties of the projection. Firstly, since the graph Γ is inscribed on the curve $P(z, w) = 0$, the image of this graph is restricted to the interior of the alga projection of this curve. Thus, the graph of the dimer model cannot be embedded arbitrarily within the T^2, but must lie within the subset of T^2 defined by the alga projection of the curve.

Secondly, we show that the allowed deformations of the graph in T^2 are restricted (in particular, arbitrary deformations of the (p, q) cycles are not allowed). Let us consider more closely the effect on the alga projection of deforming the contours. Above we showed that a contour very close to a (p, q) puncture projects to a straight line on the alga with (p, q) winding number. It is also true that *any* choice of contour encircling a puncture of $P(z, w) = 0$ maps to a cycle with the same (p, q) winding number in the alga,

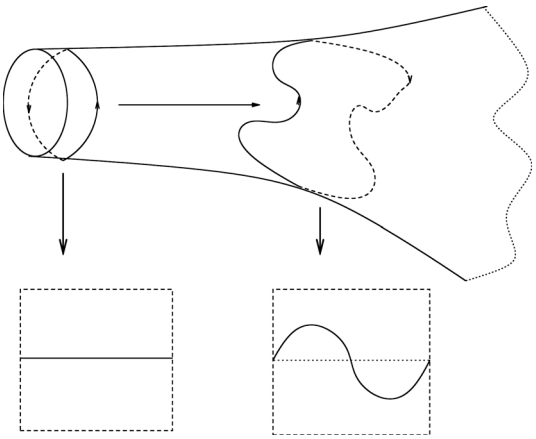

Figure 18: Two choices of contour encircling a puncture on the curve Σ. Far along the cylinder, i.e., close to the puncture, the contour projects to a straight line in the angular T^2. When this contour is deformed, the projection to the T^2 is also deformed, but it is not translated in the torus and has the same average position.

since they are related by continuous deformations. Moreover, deforming the choice of contour on Σ does not change the average position of the projection to the alga (i.e., does not produce a translation of the winding path on the torus). The allowed projections of contours to the alga are therefore constrained by the moduli of the curve, see figure 18. Let us now show this fact.

Without loss of generality, we may consider the puncture to be a cylinder aligned in the $(-1, 0)$ direction (any other choice of orientation is related by an $\mathrm{SL}(2, \mathbb{Z})$ transformation). The location of the puncture is therefore at the point $z = 0$ on Σ (i.e., $\log|z| \to -\infty$), and a contour very close to the puncture projects to a horizontal straight line in the alga given by $\phi = \mathrm{Arg}(w) \equiv \phi_0$, a constant determined by the curve moduli, as in (7.6). For any other choice of contour, the average value of ϕ along the contour is given by

$$\begin{aligned}\overline{\phi} &= \frac{1}{2\pi\imath}\oint_{z=0} \mathrm{Arg}(w(z))d(\log z) \\ &= \frac{1}{2\pi\imath}\oint_{z=0} \mathrm{Arg}(w(z))\frac{dz}{z} \\ &= \mathrm{Arg}(w(0)) \\ &= \phi_0 \end{aligned} \tag{7.7}$$

as long as the puncture is isolated, i.e., two punctures do not collide.

7.3 Projection of the D6-branes

As we discussed in Section 3, the wrapped D6-branes that provide a basis for the quiver correspond to 1-cycles on the curve Σ that wind the cycles which vanish at critical points in the W-plane. Under the untwisting map the discs attached with boundary along these 1-cycles map to the faces of the dimer model on T^2. We will later show in several examples that under the (alga) T^2 projection to phases of (z, w) these vanishing cycles also map to the faces of the dimer model.

Taking $W = P(z, w)$, critical values of W define points where the curve fibre degenerates, i.e., a certain homology 1-cycle of the curve $P(z, w) = W$ vanishes. At this point, the vanishing 1-cycle collapses to a point, and therefore the projection of the cycle to the alga is also a point. As we move away from this point by changing W, this point will resolve into a circle, which will project to a small closed circle in the alga also. Along the straight-line path from the critical point $W = W_*$ towards $W = 0$, the vanishing cycle sweeps out a closed disc in the angular T^2.

Multiple such straight-line paths all meet at $W = 0$. Thus, near $W = 0$, where the discs are attached along the S^1 paths along the graph Γ, which projects to the graph of the dimer model, the disc swept out by the vanishing cycle in the T^2 approaches the piecewise linear polygonal face of the dimer model. Hence, the image of the vanishing cycles along the straight-line paths projects to the *closed* polygonal faces of the dimer model. Let us now enlighten the reader with some illustrative examples.

7.4 Examples

7.4.1 $\mathbb{C}^3$

If one prescribes an embedding of the graph of the dimer model within the alga projection of the curve $P(z, w) = 1 - w - z = 0$ (i.e., prescribing the angular parts of z, w), it is straightforward to solve for the absolute values to lift this to an embedding of the graph Γ on the curve.

Writing

$$z = Ae^{\imath\theta}, \quad w = Be^{\imath\phi} \tag{7.8}$$

and setting the real and imaginary parts of $P(z, w)$ to zero, we find

$$A = -\frac{\sin(\phi)}{\sin(\theta - \phi)}, \quad B = \frac{\sin(\theta)}{\sin(\theta - \phi)} \tag{7.9}$$

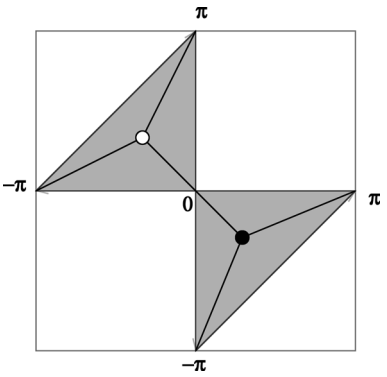

Figure 19: An embedding of the dimer model for $\mathbb{C}^3$. The shaded region is the alga projection of the curve $P(z,w) = 1 - z - w = 0$, and in this case it is bounded by the straight-line winding cycles with $(p,q) = (1,1), (-1,0), (0,-1)$.

If one chooses the two vertices of the dimer model to be located at $\pm(-\pi/3, \pi/3)$ and connected by straight lines (see figure 19), the graph of the dimer model on T^2 may be parametrized by the 3 paths:

$$\begin{aligned}
\theta_1(t) &= -\frac{\pi}{3} + \frac{2\pi}{3}t, \quad \phi_1(t) = \frac{\pi}{3} - \frac{2\pi}{3}t; \\
\theta_2(t) &= \frac{\pi}{3} + \frac{4\pi}{3}t, \quad \phi_2(t) = -\frac{\pi}{3} + \frac{2\pi}{3}t; \\
\theta_3(t) &= -\frac{\pi}{3} + \frac{2\pi}{3}t, \quad \phi_3(t) = \frac{\pi}{3} + \frac{4\pi}{3}t,
\end{aligned} \tag{7.10}$$

where $t \in [0,1)$. Substituting these paths into (7.9) parametrizes an embedding of the graph Γ into the curve $P(z,w) = 0$. Since this curve has real coefficients, it is Harnack, and the amoeba projection is simple (see Section 6.1.2) (recall each point on the interior of the amoeba lifts to two points on the curve). The amoeba projection of Γ is shown in figure 20. We see that this graph agrees with the one obtained in Section 5.1.1 by the untwisting method (see also figure 17).

Note that even though we cannot be completely explicit about the topology of the D6-branes in the full CY geometry (since Σ has genus 0 and the corresponding $W = P(z,w)$ does not have enough critical points to use the method described in Section 2.1), we see that we still obtain the full quiver theory from self-intersections of a closed path on the curve $P(z,w) = 0$ (the zig-zag path on the graph Γ, as shown in figure 11). This 1-cycle should be thought of as the intersection of the D6-brane with the curve $P(z,w) = 0$.

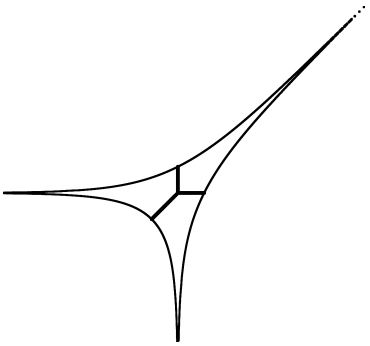

Figure 20: The amoeba projection of the graph Γ on the curve $P(z,w) = 1 - z - w = 0$ for $\mathbb{C}^3$, obtained by solving for the absolute values of z, w along the locus prescribed in figure 19. This Γ agrees with the graph obtained by untwisting, see figure 13.

7.4.2 Conifold

For simplicity we take $P(z,w) = 1 - z - w - e^t zw$ with t real. One may again solve for the absolute value of z, w in terms of the angular parts, but the expressions are more complex since P is quadratic (figure 21). Instead of writing these out we simply plot the result in figure 22: since we have chosen t real, the amoeba projection again gives a nice representation of the data, and one can verify that the lift of the graph of the dimer model is again isomorphic to the graph obtained by untwisting in Section 5.1.1, see figure 12. As in the previous example, we obtain the full quiver theory from the intersection of the D6-branes with the curve $P(z,w) = 0$.

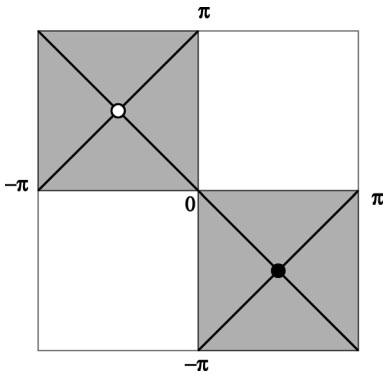

Figure 21: An embedding of the dimer model for the conifold. The shaded region is the alga projection of the curve $P(z,w) = 0$, and in this case it is bounded by the straight-line winding cycles with $(p,q) = (1,0), (-1,0), (0,1), (0,-1)$.

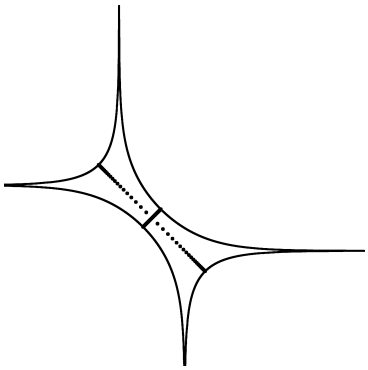

Figure 22: The amoeba projection of the graph Γ on the curve $P(z,w)=0$, obtained by solving for the absolute values of z,w along the locus prescribed in figure 21. This Γ agrees with the graph obtained by untwisting, see figure 12.

For more general curves $P(z,w)$, it is necessary to take complex moduli in order to inscribe a non-degenerate version of the dimer model graph. One may in principle still solve for the absolute values of z,w to lift the dimer model graph to a graph on the curve, but since P is no longer Harnack, the amoeba projection does not give a nice projection of this graph.

We now show in several higher-genus examples that the critical points of W correspond to the faces of the dimer model, in agreement with the general proposal.

7.4.3 $\mathbb{C}^3/\mathbb{Z}_3$

$$P(z,w)=1+z+w+\frac{e^t}{zw} \tag{7.11}$$

Critical points of $W=P(z,w)$ are obtained when $z=w=\lambda e^{t/3}$, with $\lambda^3=1$. The critical values are $W_*=1+3\lambda e^{t/3}$. We show this in part (a) of figure 24.

Thus, there are three wrapped D6-branes, corresponding to the 3 gauge groups in the quiver. The vanishing cycles are located at $z=w=\lambda e^{t/3}$, which project to the points $(0,0)$, $(2\pi/3,2\pi/3)$, $(4\pi/3,4\pi/3)$ in the alga. These are indeed the centre of the hexagonal faces in the graph of the dimer model, see figure 23. As one proceeds from $W=0$ to critical points in a straight line, faces of the dimer model get filled in, see parts (b) and (c) of figure 24.

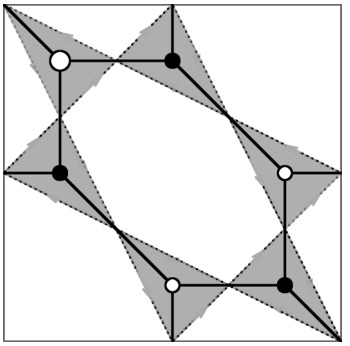

Figure 23: The dimer model for $\mathbb{C}^3/\mathbb{Z}_3$. The shaded region is the alga projection of the curve, and in this case it is bounded by the straight-line winding cycles with $(p,q) = (1,1), (-2,1), (1,-2)$, which form triangular regions. The graph of the dimer model describing the quiver theory of $\mathbb{C}^3/\mathbb{Z}_3$ may be inscribed within these triangular regions, as shown.

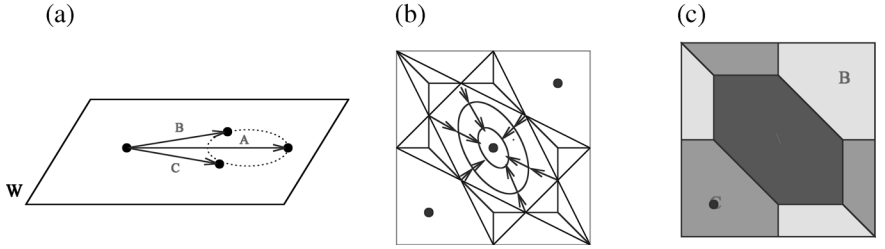

Figure 24: (a) For $\mathbb{C}^3/\mathbb{Z}_3$, there are 3 critical points in the W-plane; (b) The alga projection of the critical values of z, w at the critical points of W are in the interior of the three hexagonal faces of the dimer graph. Along the straight-line paths from $W = 0$ to a critical point, the corresponding face of the dimer model fills in. (c) The combination of these paths fills the entire T^2 in the angular parts of z, w. The S^1 fibre in the uv-plane vanishes over the boundary of each face and is non-vanishing in the interior, which exhibits these faces as the S^3 wrapped branes.

7.4.4 $Y^{3,1}$

The spaces $Y^{p,q}$ have recently been much studied. Let us focus on $Y^{3,1}$. The toric diagram and the corresponding $P(z,w)$ are

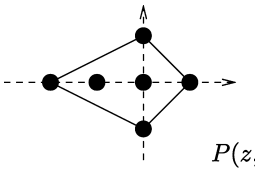

$$P(z,w) = 1 + z + \frac{e^{-a}}{z} + \frac{e^{-b}}{z^2} + w + \frac{e^{-c}}{w} \tag{7.12}$$

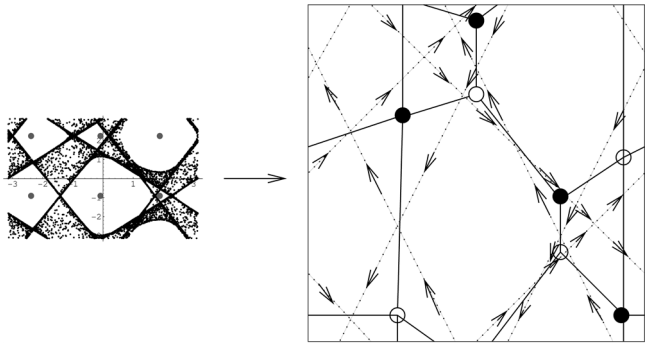

Figure 25: The alga for $P(z,w) = 1 + z + \frac{1+\imath}{z} + \frac{3-2\imath}{z^2} + w + \frac{-1-4\imath}{w}$. Critical values of z, w are marked by red dots in the alga projection. The straight line (p,q) winding cycles are visible as accumulation points, the projection of points lying along the half-cylinders. This geometrical data is consistent with the dimer model shown.

Indeed, the toric diagram contains 2 internal points, so the Newton polynomial defines a genus 2 curve in the mirror geometry.

There are generically six critical points of $W = P(z,w)$ by the arguments of appendix A. In figure 25 we plot the alga of $P(z,w)$ with randomly chosen values of the moduli $(e^{-a} = 1 + \imath, e^{-b} = 3 - 2\imath, e^{-c} = -1 - 4\imath)$, and the location of the corresponding critical values of z, w. We may inscribe a dimer model within the alga projection of the curve such that these points lie within the faces of this dimer model. This dimer model is also consistent with the straight-line (p,q) winding paths, which are shown. In this case the straight line paths bound regions enclosing the vertices with alternating orientations, so the dimer model is easy to read off. In general this may not be true, although based on the argument in Section 7.1 (see also Section 4.3) one can always deform these straight-line paths to meet at vertices while keeping the same average value.

In figure 26 the straight line paths from $W = 0$ to the critical points $W = W_*$ are shown. The alga projection of $P(z,w) = W_*$ shows the vanishing cycle located at the critical values, since the corresponding face of the dimer model fills in along this path.

7.5 Degenerations

Since the T^2 is only a projection onto a half-dimensional subspace, various things may go wrong with the image of this projection. We discuss some of them, although we do not study these degenerations in detail.

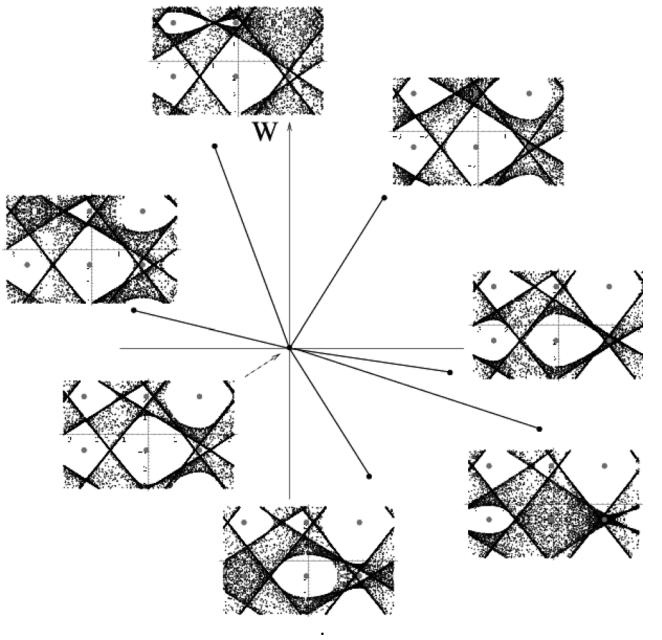

Figure 26: By plotting the alga projection of the curve $P(z, w) = W$ we see that near the critical points W_* the alga fills in the region of the vanishing cycle (critical values of z, w, marked with red dots). Thus, the vanishing cycles sweep out the faces of the dimer model shown in figure 25.

When $P(z, w) = 0$ is a Harnack curve, i.e., when the coefficients of P are real, the amoeba map has the property that the boundary of the amoeba is also real. This is maximally nice from the point of view of the amoeba, but maximally bad from the point of view of the alga, since it means that on the boundary of the fundamental domain the image of the curve contracts to the points $(0, 0), (0, \pi), (\pi, 0), (\pi, \pi)$.

Thus, *any* contour that touches the boundary of the amoeba (in particular, any contour that encircles a puncture on Σ, which projects in the amoeba to a line segment extending between two boundary components) passes through these degenerate points. This obscures the projection of Γ and does not produce an isomorphic graph. Taking the moduli of the curve to be generic complex numbers avoids this problem.

In principle different embeddings of Γ may produce degenerate projections to T^2, i.e., if they contain two points with the same angular parts, they will project to the same point and create "spurious vertices" in the projection of Γ.

However, we conjecture that it is always possible to find situations where the projection is non-degenerate (by adjusting the moduli of the curve $\Sigma : P(z, w) = 0$ and/or by deforming the embedding of $\Gamma \subset \Sigma$). As in the examples discussed in the previous section, when the alga is suitably non-degenerate one may inscribe the desired dimer graph in the interior of the alga projection (which prescribes the angular parts of z, w along Γ) and solve for $|z|, |w|$ to map the dimer graph to Γ (by definition of the alga projection, a solution exists on the curve). This constructs a Γ that is graph-isomorphic to the dimer graph T^2.

In such cases, the dimer models in T^2 are obtained by projection of Γ. In general it is simpler to consider the dimer model on Γ itself, or to use the twisting map to relate it topologically to a graph on T^2 without having to worry about a choice of embedding. Considering the specific projection to angular variables imposes restrictions on the image in T^2 and may provide further information. This problem should be studied in more detail.

7.6 Seiberg duality from algæ

Now we discuss Seiberg duality from the point of view of alga projections. As we have shown [4, 17] and discussed in Section 5.4, Seiberg duality is the result of PL transformations, where one cycle passes over another. More concretely, $P(z, w) - W = 0$ gives various critical points in the W-plane and the bases S^3 of the third-homology are given by straight lines in the W-plane connecting the origin to these critical points.

As we vary moduli (coefficients in $P(z, w)$), the positions of critical points change correspondingly. Hence, it is clear that sometimes one straight line will pass another straight line, whereby inducing the PL transformation. From the point of view of the actual geometry, such a transformation is non-trivial. We would thus like to see that after the alga projection, how this effect shows up in the dimer model. One possible way is illustrated by the following.

Let us again exemplify using the Hirzebruch-zero geometry F_0. The curve, rescaling (2.3), is given by

$$P_{F_0}(z, w) = k - z - 1/z - w - e/w$$

where k, e are complex moduli. Now let us study how phases change when we vary the moduli. To do this we have chosen $k = 3 + 3i$ and $e = 2 + i\alpha$ with α varying. We choose four cycles, corresponding to the four legs (spines), parametrized as $z = r_0 e^{it}$ with $t \in [-\pi, +\pi]$ and such that $r_0 = e^3$ for cycles $(1, \pm 1)$ and $r_0 = e^{-3}$ for cycles $(-1, \pm 1)$.

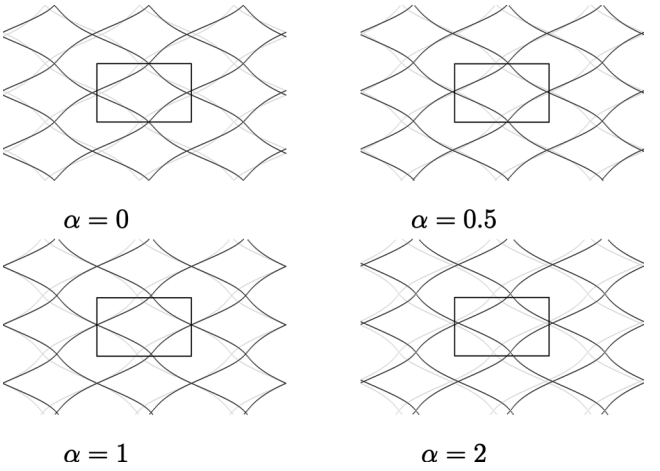

Figure 27: The 4 S^1s winding the four cylinders of F_0 under the alga projection. We vary the parameter α which represents a complex modulus of Σ and see how the intersection varies for four different values of α as indicated. The fundamental domain $[-\pi, \pi]$ is indicated by the black box.

We now follow how these four cycles project in the alga and the results are given in parts (a), (b), (c) and (d) of figure 27. To see the periodicity of the alga projection more clearly, we draw in 3×3 times the fundamental unit, which is indicated in the black square.

Now we can see how the intersection of the four cycles changes from $\alpha = 0$ to $\alpha = 2$. The main difference is that the zig-zag cycles $(1, 1)$ and $(-1, -1)$ do not intersect at $\alpha = 2$, but do have two extra intersections at $\alpha = 0$, one with plus and one with minus sign, so the topological intersection number is still zero from the perspective of dimer. However, such "superficial" extra intersections in the dimer model is crucial for Seiberg duality because they come from the intersection in the real geometry. In other words, they are actual intersections in Σ.

It is worth to notice that at $\alpha = 1$, all four cycles intersect at the same point. Thus these two phases interpolate to each other through this degenerate point. We see that indeed for certain choices of the moduli, the projection onto the alga precisely reproduces the zig-zag paths. We conjecture similar procedures may be applied in general.

We must emphasize that the above results, though highly suggestive, are not fully right because the four contours we have chosen do not actually intersect each other in the real geometry Γ. However, we think it may give the right topological picture about Seiberg duality in the dimer model.

8 Discussion

In this paper we have studied the intersecting D6-brane systems that give rise to toric quiver gauge theories on their world-volume. We found that the intersection of the D6-branes with the curve $P(z, w) = 0$, which is part of the CY geometry $\mathcal{W}$ mirror to the original toric CY $\mathcal{M}$, encodes the matter content and tree-level superpotential of the quiver theory.

The D6-brane world-volumes form a singular T^3. In principle the singularities of this T^3 could have been of a complicated form. However, we found that for the quiver theories coming from D3-branes at the tip of toric CY cones, the only singularity of the mirror D6-branes comes from a vanishing S^1 fibre over a T^2, where the fibre vanishes along a bipartite graph[8] in T^2. This realizes the dimer models on T^2 as living on a subset of the T^3 world-volume of the D6-branes, and provides a concrete string theoretical framework for the previous combinatorial results relating dimer models and quiver gauge theories [9, 10, 29].

Here we have only discussed the *topology* of the D6-branes. From general arguments the supersymmetric D6-branes should wrap special Lagrangian cycles. Since they have topology S^3 (i.e., $b_1 = 0$) these cycles should be rigid. It would be interesting to see whether the ideas of isoradial embeddings of the dimer model graph, and the interpretation of R-charges as angles in such embeddings [29], can be fit into the present framework. Specifically, the a-maximization of angles of the graph in T^2 selects one embedding of the dimer model; is this related to the selection of the special Lagrangian cycle? Alternatively, we may be closer to the Z-minimization of [43], which is also formulated in terms of toric geometry.

It should be possible to understand these results on dimer models from intersecting D6-branes from a world-sheet perspective using linear sigma models with A-type boundary conditions. This problem is currently under investigation (K. Hori and K.D. Kennaway, Work in progress). From the target space point of view one should also be able to relate the D6-branes and associated dimer models on $\mathcal{W}$ to the mirror branes on $\mathcal{M}$, which form an exceptional collection of sheaves.

The structure governing the intersection of the D6-branes with the curve $P(z, w) = 0$ is that they form zig-zag paths on a bipartite graph Γ on the curve. This graph Γ also produces a decomposition of the curve into half-cylinders. One might imagine constructing different possible Γ by the

[8] This may have implications for the special Lagrangian fibration structure of the mirror geometry, cf. [42].

converse gluing operations; in general there is an ambiguity in how Γ may be constructed by gluing of half-cylinders (this ambiguity admits the various Seiberg-dual phases of the quiver theory). It should be possible to clarify the consistency conditions for the resulting quiver theories. It would also be interesting to understand this structure geometrically.

We were not able to be completely explicit about the D6-branes when the toric CY contains only a vanishing 2-cycle. While we still obtain the full quiver theory from intersections of 1-cycles on the curve $P(z, w) = 0$, the function $W = P(z, w)$ does not have enough critical points to treat these cases uniformly with the vanishing 4-cycle cases. See Appendix A for one idea on the resolution to this puzzle.

We introduced a projection of the mirror geometry (dubbed the alga projection) that produces the dimer models on T^2 in suitable cases. This projection has not been well studied by mathematicians, so further study of the properties of this projection and its relation to dimer models is needed.

Now that we have understood the role of dimer models in describing the tree-level superpotential of the quiver theories, can we also use the dimer models as a basis for studying quantum corrections? It is already known [16] (see also [44, 45]) that these same dimer models may be used to compute the topological string partition function, so it is likely that the answer is yes.

Acknowledgments

B.F. gratefully acknowledges Marie Curie Research Training Network under contract number MRTN-CT-2004-005104 and the IAS, Princeton under NSF grant PHY-0070928; he extends his thanks to the Universities of Amsterdam, Durham and Oxford for their hospitality. Y.H.H. is indebted to the patronage of Merton College, Oxford (especially to the Rt. Rev. Warden Richard FitzJames, Bishop of London) as well as the Mathematical Institute of Oxford University; he would also like to express his sincere gratitude to the Department of Physics (DE-FG02-95ER40893) and the Math/Physics RG (NSF-DMS0139799 Focused Grant for "The Geometry of Strings") at the University of Pennsylvania where this work began and for three happy years past. K.K. is supported by NSERC, and thanks Alastair Craw, Jarah Evslin, Manfred Herbst, Kentaro Hori, Robert Karp, David Page, Christian Römelsberger and James Sparks for enlightening discussions, and the Fields Institute and Department of Physics at the University of Toronto for support; he also is grateful to Harvard University, and the University of Pennsylvania for being warm hosts. CV is supported in part by

NSF grants PHY-0244821 and DMS-0244464. B.F., Y.H.H. and K.K. jointly thank Sebastian Franco, Amihay Hanany, David Vegh and Brian Wecht and the kind hospitality of MIT. K.K. and C.V. thank the Simons Workshop in Mathematics and Physics, Stony Brook for providing a stimulating and productive environment.

Appendix A Number of critical points of $P(z, w)$ and the Newton polytope

In this Appendix, we show that the number of critical points of $W = P(z, w)$ is equal to twice the area of the toric diagram, which in turn is equal, by (5.2), to the number of gauge groups in the quiver.

First, there are some nice theorems on the relationship between the number of solutions of polynomial systems and the Newton polytope spanned by the polynomials, culminating in the Koushnirenko–Bernstein theorem [46, 47] (for relations to amoebæ, q.v. [21, 48]):

> *The number of joint zeros in* $(\mathbb{C}^*)^m$ *of* m *generic polynomials* $\{f_1, f_2, \ldots f_m\}$ *with a given Newton polytope* Δ *is equal to* $m!\mathrm{Vol}(\Delta)$.

The case at hand has $m = 2$, with the equation system being

$$\left\{ \frac{\partial P(z,w)}{\partial z}, \frac{\partial P(z,w)}{\partial w} \right\} = 0. \tag{A.1}$$

Now, the Newton polytopes of $\frac{\partial P(z,w)}{\partial z}$, $\frac{\partial P(z,w)}{\partial w}$ and $P(z, w)$ are all different; however, a simple transformation would make the theorem applicable. We note that the Newton polytope of $z\frac{\partial P(z,w)}{\partial z}$ is the same as that of $P(z, w)$ except that the w-axis is deleted. Similarly $w\frac{\partial P(z,w)}{\partial w}$ has the z-axis deleted. Thus, as long as the origin (common to both axes) is an *interior* point of $P(z, w)$, i.e., when genus is greater than 0, $z\frac{\partial P(z,w)}{\partial z}$ and $w\frac{\partial P(z,w)}{\partial w}$ span the Newton polygon of $P(z, w)$ (the only point missing is the constant term, which is interior to the polygon and thus included in the convex hull). Then, the system

$$\begin{aligned} P1(z,w) = az\frac{\partial P(z,w)}{\partial z} + bw\frac{\partial P(z,w)}{\partial w} = 0; \quad P2(z,w) = az\frac{\partial P(z,w)}{\partial z} \\ + bw\frac{\partial P(z,w)}{\partial w} = 0 \end{aligned} \tag{A.2}$$

for $a, b, c, d \neq 0$ and $\det \begin{pmatrix} a & b \\ c & d \end{pmatrix} \neq 0$ has the same number of solutions as the desired (A.1) while $P1$ and $P2$ both have the same Newton polytope as $P(z, w)$.

Now, the Koushnirenko–Bernstein theorem applies and we conclude that

$$\begin{aligned} \#\text{ critical points } (P(z,w)) &= 2\,Vol(\text{ Newton Polytope of} P(z,w)) \\ &= 2\text{Area(Toric Diagram)}. \end{aligned} \tag{A.3}$$

We remark, as an aside, that we could have multiplied (A.1) by $z^s w^t$ for some sufficiently large $s, t \in \mathbb{N}$. This shift of the Newton polytope introduces extra critical points $z = 0$ or $w = 0$, which are excluded since $z, w \in \mathbb{C}^*$. Thus we could equally have run our argument above and come to the same conclusion. However, for the genus zero case, this shift does introduce valid extra solutions. Amazingly, now, we actually get the right number of critical points. However, it is not clear what this means in the geometry. Indeed, although it seems that the toric data allows us to liberally shift the origin, when we are calculating locations of critical points, results do depend on the choice of origin. The implications of this should be investigated further.

References

[1] M.R. Douglas and G.W. Moore, *D-branes, quivers, and ALE instantons*, hep-th/9603167.

[2] M.R. Douglas, B.R. Greene and D.R. Morrison, *Orbifold resolution by D-branes*, Nucl. Phys. **B506** (1997) 84–106, hep-th/9704151.

[3] K. Hori, A. Iqbal and C. Vafa, *D-branes and mirror symmetry*, hep-th/0005247.

[4] A. Hanany and A. Iqbal, *Quiver theories from D6-branes via mirror symmetry*, JHEP **04** (2002) 009, hep-th/0108137.

[5] M. Wijnholt, *Large volume perspective on branes at singularities*, Adv. Theor. Math. Phys. **7** (2004) 1117–1153, hep-th/0212021.

[6] F. Cachazo, B. Fiol, K.A. Intriligator, S. Katz and C. Vafa, *A geometric unification of dualities*, Nucl. Phys. **B628** (2002) 3–78, hep-th/0110028.

[7] B. Feng, A. Hanany and Y.-H. He, *Phase structure of D-brane gauge theories and toric duality*, JHEP **08** (2001) 040, hep-th/0104259.

[8] B. Feng, A. Hanany and Y.-H. He, *D-brane gauge theories from toric singularities and toric duality*, Nucl. Phys. **B595** (2001) 165–200, hep-th/0003085.

[9] A. Hanany and K.D. Kennaway, *Dimer models and toric diagrams*, hep-th/0503149.

[10] S. Franco, A. Hanany, K.D. Kennaway, D. Vegh and B. Wecht, *Brane dimers and quiver gauge theories*, hep-th/0504110.

[11] S. Franco, A. Hanany, F. Saad and A.M. Uranga, *Fractional branes and dynamical supersymmetry breaking*, hep-th/0505040.

[12] S. Benvenuti and M. Kruczenski, *Semiclassical strings in Sasaki–Einstein manifolds and long operators in $\mathcal{N}=1$ gauge theories*, hep-th/0505046.

[13] S. Benvenuti and M. Kruczenski, *From Sasaki–Einstein spaces to quivers via BPS geodesics: $L(p,q,r)$*, hep-th/0505206.

[14] S. Franco, A. Hanany, D. Martelli, J. Sparks, D. Vegh and B. Wecht, *Gauge theories from toric geometry and brane tilings*, hep-th/0505211.

[15] A. Butti and A. Zaffaroni, *R-charges from toric diagrams and the equivalence of a-maximization and Z-minimization*, hep-th/0506232.

[16] A. Okounkov, N. Reshetikhin and C. Vafa, *Quantum Calabi–Yau and classical crystals*, hep-th/0309208.

[17] B. Feng, A. Hanany, Y.H. He and A. Iqbal, *Quiver theories, soliton spectra and Picard–Lefschetz transformations*, JHEP **02** (2003) 056, hep-th/0206152.

[18] K. Hori and C. Vafa, *Mirror symmetry*, hep-th/0002222.

[19] K. Hori, S. Katz, A. Klemm, R. Pandharipande, R. Thomas, C. Vafa, R. Vakil and E. Zaslow, eds, *Mirror symmetry*, Clay Mathematics Monographs, **1**, AMS, Providence, RI, 2003.

[20] A. Strominger, S.-T. Yau and E. Zaslow, *Mirror symmetry is T-duality*, Nucl. Phys. **B479** (1996) 243–259, hep-th/9606040.

[21] G. Mikhalkin, *Real algebraic curves, the moment map and amoebas*, Ann. Math. **2** (2000) 151, arXiv:math/0010018.

[22] A.G. Khovanskii, *Newton polyhedra and toric varieties, Funkcional. Anal. i Prilozen* **11** (1977), 56–64.

[23] O. Aharony, A. Hanany and B. Kol, *Webs of (p,q) 5-branes, five dimensional field theories and grid diagrams*, JHEP **01** (1998) 002, hep-th/9710116.

[24] N.C. Leung and C. Vafa, *Branes and toric geometry*, Adv. Theor. Math. Phys. **2** (1998) 91–118, hep-th/9711013.

[25] R. Kenyon, A. Okounkov and S. Sheffield, *Dimers and amoebae*, arXiv:math-ph/0311005.

[26] R. Kenyon, *An introduction to the dimer model*, arXiv:math.CO/0310326.

[27] P. Kasteleyn, *Graph theory and crystal physics*, Graph theory and theoretical physics, Academic Press, London, 1967, 43–110.

[28] R. Kenyon and J.-M. Schlenker, *Rhombic embeddings of planar graphs with faces of degree 4*, arXiv:math-ph/0305057.

[29] A. Hanany and D. Vegh, *Quivers, tilings, branes and rhombi*, hep-th/0511063.

[30] B. Feng, A. Hanany, Y.-H. He and A.M. Uranga, *Toric duality as Seiberg duality and brane diamonds*, JHEP **12** (2001) 035, hep-th/0109063.

[31] G. Pick, *Geometrisches zur zahlenlehre*, *Sitzungber.* Lotos **19** (1899), 311.

[32] S. Lins, *Graphs of maps*, math.CO/0305058. PhD Thesis.

[33] M. Berkooz, M.R. Douglas and R.G. Leigh, *Branes intersecting at angles*, Nucl. Phys. **B480** (1996) 265–278, hep-th/9606139.

[34] M. Aganagic, A. Karch, D. Lust and A. Miemiec, *Mirror symmetries for brane configurations and branes at singularities*, Nucl. Phys. **B569** (2000) 277–302, hep-th/9903093.

[35] S. Franco and A. Hanany, *Geometric dualities in 4d field theories and their 5d interpretation*, JHEP **04** (2003) 043, hep-th/0207006.

[36] B. Feng, Y.-H. He and F. Lam, *On correspondences between toric singularities and (p,q)-webs*, Nucl. Phys. **B701** (2004) 334–356, hep-th/0403133.

[37] B. Feng, S. Franco, A. Hanany and Y.-H. He, *Symmetries of toric duality*, JHEP **12** (2002) 076, hep-th/0205144.

[38] G. Mikhalkin, *Amoebas of algebraic varieties and tropical geometry*, arXiv:math.AG/0403015.

[39] G. Mikhalkin, *Amoebas of algebraic varieties*, arXiv:math.AG/0108225.

[40] H. Rullgård, *Topics in geometry, analysis and inverse problems*, PhD Thesis, Dept. Math., Univ., Stockholm, 2003.

[41] A. Harnack, *Über vieltheiligkeit der ebenen algebraischen curven*, Math. Ann. **10** (1876) 189–199.

[42] M. Gross, *Examples of special Lagrangian fibrations*, arXiv:math.AG/0012002.

[43] D. Martelli, J. Sparks and S.T. Yau, *The geometric dual of a-maximisation for toric Sasaki–Einstein manifolds*, hep-th/0503183.

[44] J. Stienstra, *Mahler measure variations, Eisenstein series and instanton expansions*, arXiv:math.NT/0502193.

[45] J. Stienstra, *Mahler measure, Eisenstein series and dimers*, arXiv:math.NT/0502197.

[46] A.G. Koushnirenko, *Polyhédres de Newton et nombres de Milnor*, Inv. Math. **32** (1976), 1–31.

[47] D. Bernstein, *The number of roots of a system of equations*, *Funct. Anal. App.* **9(2)** (1975), 183–185.

[48] B. Shiffman and S. Zelditch, *Random polynomials with prescribed Newton polytope, I* arXiv:math/0203074.